

Simulating the Electron Optics of an Electron Beam Manufacturing 3D Printer

Using COMSOL Multiphysics® to Simulate the Electron Beam Trajectories in the Magnetic Lens System of an Arcam EBM 3D Printer

MARTIN GARDFJELL

Date: August 17, 2020

MASTER'S THESIS

Simulating the Electron Optics of an Electron Beam Manufacturing 3D Printer

Using COMSOL Multiphysics® to Simulate the Electron
Beam Trajectories in the Magnetic Lens System of an
Arcam EBM 3D Printer

MARTIN GARDFJELL



CHALMERS
UNIVERSITY OF TECHNOLOGY

Department of Physics
CHALMERS UNIVERSITY OF TECHNOLOGY
Gothenburg, Sweden 2020

Simulating the Electron Optics of an Electron Beam Manufacturing 3D Printer
Using COMSOL Multiphysics® to Simulate the Electron Beam Trajectories in the
Magnetic Lens System of an Arcam EBM 3D Printer

MARTIN GARDFJELL

© MARTIN GARDFJELL, 2020.

Supervisor: David Svensson, GE Additive
Examiner: Paolo Vinai, Department of Physics, Chalmers

Master's Thesis 2020
Department of Physics
Chalmers University of Technology
SE-412 96 Gothenburg
Telephone +46 31 772 1000

Cover: The particle trajectories of a few selected electrons propagating through a
Magnetic Lens System with a focus lens and a deflections lens.
Modelled in COMSOL Multiphysics®.

Typeset in L^AT_EX
Printed by Chalmers Reproservice
Gothenburg, Sweden 2020

Simulating the Electron Optics of an Arcam Electron Beam Manufacturing 3D Printer

Using COMSOL Multiphysics® to Simulate the Electron Beam Trajectories in the Magnetic Lens System of an Arcam EBM 3D-printer

MARTIN GARDFJELL

Department of Physics

Chalmers University of Technology

Abstract

Additive Manufacturing (AM) is a growing industry that has the potential to completely revolutionize global manufacturing. Electron Beam Manufacturing (EBM) is a 3D-printing method developed by GE Additive that utilizes an electron beam, controlled by a magnetic lens system, to melt metal powder. GE is currently looking into opportunities for simulating the Electron Optics, with the ambition to further develop their EBM technology. In this project a model of the lens system has been built and evaluated in COMSOL Multiphysics®. Using the Finite Element Method (FEM) and Time Step Particle Tracing it was possible to simulate the electron trajectories in 25 min. The computational time was substantially reduced by approximating certain calculations and replacing COMSOL's default Generalized Alpha Time Stepping algorithm with a simpler algorithm in certain regions. The accompanied decrease in accuracy was negligible compared to the error in the model itself, proving that there is a lot of potential for improvement. The thesis concludes that COMSOL is a useful FEM software for simulating the electron optics of an Arcam EBM lens system. The model created in this thesis does however require further development, especially regarding mesh convergence, before the software can be implemented as a simulation tool at GE Additive.

Keywords: Computational Electromagnetics, Electron Optics, Charged Particle Optics, Additive Manufacturing, Arcam Electron Beam Manufacturing, GE Additive, COMSOL Multiphysics®, Finite Element Method, Boundary Element Method, Generalized Alpha

Acknowledgements

First of all I would like to thank my supervisor David Svensson for all his support in this project. He was able to tailor this project to fit my own and the companies needs very well. I would also like to thank him, and the rest of the people in the team for making me feel like a part of GE Additive. It was a shame that the team had to work from home due the Covid-19 outbreak, because I really enjoyed working with them. Calle Hellestam was the first person I got in contact with when applying to do the thesis and he has looked after me ever since. He has supported me throughout the project and supplied me with all the tools I could possibly need to succeed. A lot of gratitude also goes out to the rest of the staff at GE Additive whom I've interacted with throughout the months. It has been a true pleasure to work at such a fantastic company!

I would also to thank Paolo Vinai for being my examiner. I have always felt encouraged by him and his feedback is always spot on. His support has been empowering and helped me a great deal in this project.

Lastly a would like to thank Björn Bragée and the people working in the COMSOL Support for tirelessly answering my endless amount of questions.

Martin Gardfjell, Gothenburg, June 2020

Contents

List of Figures	xi
List of Tables	xiii
1 Introduction	1
1.1 Background	1
1.2 Scope and Structure of the Thesis	3
1.3 Ethical, Societal and Environmental concerns	4
2 Theory	5
2.1 Arcam EBM Technology	5
2.1.1 Electron Source	6
2.1.2 Electron-Powder Interaction	6
2.2 Electron Optics	7
2.2.1 Beam Properties	7
2.2.2 Electron-electron interaction	9
2.3 Magnetic fields and Magnetic Lens Design	10
2.3.1 The Focus Lens	12
2.3.2 The Deflection Lens	13
2.3.3 The Astigmatism Lens	15
2.4 Numerical Methods	16
2.4.1 Finite Element Method	17
2.4.1.1 Mesh optimization	18
2.4.2 Particle Trajectory Calculations with Time Stepping	20
2.4.2.1 The Generalized Alpha Method	20
2.4.3 Quadratic Trajectory Fitting	22
3 Methodology	23
3.1 Delimitations	23
3.2 The COMSOL model	24
3.3 Mesh Convergence and Model Evaluation	27
3.3.1 Mesh Design	27
3.3.2 Mesh Evaluation	29
3.3.3 Computational Time	31
3.4 Methods to reduce the computational time	32
3.4.1 Super-positioning the magnetic fields	32
3.4.2 Approximating the electric field	32

3.4.3 Customizing the Time Step Algorithm	34
4 Results	37
5 Conclusions and Recommendations	41
5.1 Discussion	41
5.2 How fast is fast enough?	43
5.3 Conclusion	44
Bibliography	46
A Electron Source Specifications	I

List of Figures

2.1	Schematic of the entire Arcam EBM machine.	5
2.2	Hyperemittance (top), Emittance (middle) and Brightness (bottom) for the cross-section of a beam when it is Converging, Focused and Diverging.	9
2.3	The electron-electron interaction between two infinite parallel currents $I = nq_ev$ a distance r apart. For $v = c/2$ the magnetic force per unit length F_B can be found to be a quarter of the electric force per unit length F_E	10
2.4	The magnetic fields created by a straight wire and a circular wire. The darker color indicates a stronger magnetic field strength and the arrows indicate the direction of the field.	11
2.5	A schematic of the magnetic field B created by a solenoidal with five turns and how electrons with and without initial angles interact with it. The wavy trajectory of the angled electron represents the spiraling effect associated with the convergence.	12
2.6	Deflection of an electron in a homogeneous magnetic field.	13
2.7	Four models of deflection lenses of increasing complexity. From left to right: a Helmholtz coil, a modified Maxwell coil, a square modified Maxwell coil and a Saddle Coil. All coils approximate a homogeneous magnetic field.	14
2.8	The design and layout of a 24 th order Saddle Coil. The left schematic displays a top view of the coil and how the vertical wires (circles) and circle segments (arcs) are indexed. The dashed lines show which vertical wires are directly connected when creating a magnetic field in the x-direction and the dotted for the y-direction. The right figure shows a 3-dimensional view of the deflection coil in COMSOL.	15
2.9	Deflection lens (left) and astigmatism lens (right).	16
2.10	A simplified illustration of how a target function $f(x)$ can be numerically approximated on a 1-dimensional domain x	17
3.1	Geometry of the system.	24
3.2	The magnetic field created by the lens system. The flux density is largest in the red regions surrounding the lens system and the white streamlines visualize the magnetic field line.	25
3.3	Particle Trajectories. The colors indicate the magnitude of the force exerted on the particles, which is strongest in the lens system.	26

3.4	The Electric Potential created from the charge distribution of the particle trajectories.	27
3.5	The three mesh designs: Default (bottom left), Only Foil (bottom right) and Foil & Intermediate (top).	28
3.6	The results from the mesh convergence for the Only Foil design (top) and Foil & Intermediate design (bottom), using convergence variable Δr , FWHM and E_B . The dotted data represent the Default design in both graphs.	29
3.7	A robustness study that introduces random points (500 per iteration) in the mesh.	30
3.8	Time evaluation of simulation number 8.	31
3.9	The radial Electric Potential $V(r, z)$ and the radial Electric Field $E_r(r, z) = -\nabla V$ created by a straight electron beam traversing down the optical axis. Notice how the electric potential falls in the foil region due to the foil being grounded.	33
3.10	The average radial Electric Force F_E (blue line) of a straight beam can be seen to increase almost linearly up until $r \approx 10$ mm, whereafter it approaches zero slowly. The scatter plots shows the electric forces exerted on 100 particles at 14 different time steps between $z = 600$ mm and $z = 1000$ mm. The different colored clusters represent different z-positions.	34
3.11	The linear propagation error accumulated propagating from, or to, the position z_i	35
4.1	Hyperemittance in the focal and offset planes for the true, linear and for the Velocity Verlet time step propagation, both with and without deflection.	39
A.1	Histogram of the initial position and velocity of the electron source.	I

List of Tables

3.1	COMSOL's nine default sets of values for the meshing parameters hmax, hmin and hgrowth. The values for hmax and hmin are given in millimeters.	28
3.2	Detailed information regarding the models used in the mesh convergence test for both the Only Foil design (top) and Foil & Intermediate design (bottom)	30
3.3	Meshing parameter values in the three regions for simulation number 8 (Foil & Intermediate). Finest Default included as reference.	31
4.1	Average positional displacement Δr and FWHM ,for short and long axis, for the hyperemittance in the focal and offset plane for the true propagation, the linear propagation and the velocity verlet propagation.	40

Abbreviations

AM	Additive Manufacturing
BEM	Boundary Element Method
EBM	Electron Beam Manufacturing
FEM	Finite Element Method
FWHM	Full Width Half Max
GE	General Electric
PCA	Principle Component Analysis

Nomenclature

a	Particle acceleration
α_m, α_f	Alpha parameters
B	Magnetic Flux Density
H	Magnetic Field Strength
c	Speed of light
D	Electric Displacement
Δr	Average positional displacement
Δt	Timestep
E	Particle energy
E	Electric Field Strength
E_B	Magnetic energy
ϵ	Emittance
ϵ_0	Permittivity
F	Force
$\gamma(v)$	Lorentz factor
I	Current
J	Current density
M	Magnetization
m_e	Electron mass
μ_0	Permeability
β, γ	Newmark parameters
φ	Deflection angle
p_x, p_y, p_z	Particle momentum
q_e	Electron charge
σ	Standard deviation
σ_0	Conductivity
α, β, γ	Twiss parameters
v	Particle velocity
x, y, z	Particle position

1

Introduction

Technologically advanced companies are constantly looking for approaches towards improving their products. Computer simulation is a powerful tool to quickly investigate new or existing concepts without having to invest a lot of resources into building or testing physical prototypes. It goes without saying that simulations can not completely replace physical prototyping, perfectly realistic models are simply impossible to build, however the true strength lies in combining them. By simulating a sufficiently advanced model of a system one can obtain enough information to be able to determine which physical prototypes are worth manufacturing and not. This project aims to create and evaluate a Computational Electromagnetic Model for GE Additive that simulates the Magnetic Lens System in their Arcam EBM Machines.

Arcam EBM Technology is an Additive Manufacturing (AM) method developed by GE Additive. Electron Beam Manufacturing (EBM) is a patented AM method for 3D-printing in metal. The method utilizes an electron beam to selectively melt metal powder. The success of the method highly relies in the accuracy to control the beam, which is done with a highly precise magnetic field created by a series of coils. The system of coils, together with the surrounding enclosure, make up the Magnetic Lens System. The Magnetic Lens System is fairly complex and it is not trivial to deduce the effects on the electron beam when the lens system is changed slightly. By simulating the system, insights regarding the dynamics of the system can be obtained faster than using manual experimentation, resulting in a faster development process of new lens models and prototypes.

1.1 Background

GE Additive has a lot of different customers with different needs and different versions of their Arcam EBM 3D-printing machines. As the industry progresses, so do the standards and demands of the customers. GE Additive is constantly looking to fix existing flaws, implement new features and increase the accuracy of their machines. When tasked to fix an identified problem, a skilled technician will often have a pretty good idea where to start looking for improvements, but it still takes a lot of time and resources to physically test the prototypes. The machines are very expensive and the cost of using them is quite high. Therefore it is very important that the amount of physical testing is minimized as much as possible and that the

tests themselves can be shown to be highly likely to succeed, in order to reduce the number of unsuccessful tests.

If there existed a tool for which an engineer could test a hypothesis quickly and remotely a lot of time and resources could potentially be saved. This tool is of course a simulation tool capable of modelling the lens system and propagating the electron beam through it. The engineer would load the lens design into the model and would be able to alter it in accordance to his or her hypothesis. Thereafter a series of simulations, sweeping over parameters of interest, could be evaluated and compared to real data. Hopefully the simulations will give results supporting further testing and if not they will still provide valuable information on which hypotheses are less likely to be worth prototyping. For this purpose the simulation tool should be fast and simple to use, while still maintain a sufficient accuracy and enough flexibility to be able to adapt the tool to a wide variety of issues.

Previous models of the lens system have been simulated using both the CPO [1] and Opera [2] software programs. Both the Finite element Method (FEM) and the Boundary Element Method (BEM) have been investigated as numerical methods. The FEM method works fairly well, but it is quite computationally expensive because of the large volume of the beam chamber. The chamber is several orders of magnitudes larger than the resolution necessary to model the beam. Due to this, a large error accumulates as the electron trajectories propagate through the approximated electromagnetic fields in the finite elements if the resolution is too low. However, due to a large volume of the chamber, relative to the desired resolution of the beam, a larger resolution of the chamber results in a much longer computational time. BEM on the other hand operates from a completely different mathematical framework, where the volume is not required to be divided into smaller elements. This is hypothesised to be computationally beneficial when modelling the EBM lens system.

There are some issues with the two software's currently used. CPO has been used for some time and shows good convergence for BEM calculations. However, CPO is no longer actively developed and maintained. This imposes a future risk of the program becoming obsolete and therefore the decision was made to change software. Opera was investigated at first but showed difficulties converging using BEM calculations. With a desire to model the system in BEM, GE Additive saw promise in the simulation software COMSOL Multiphysics® and therefore it was chosen as the next candidate to investigate. The initial purpose of this project was to use COMSOL to model the Magnetic Lens System. The scope of the project was set on calculating the system independently with both FEM and BEM, and thereafter to compare the FEM and BEM solvers to each other. Midway through the project it became clear that COMSOL lacked the necessary mathematical framework required by BEM to model vector based potentials, i.e. the currents in the lenses that produce the magnetic field. The scope of the project was therefore limited to only simulate FEM models and thereafter extended to investigate additional methods to lower the computational time.

1.2 Scope and Structure of the Thesis

The aim of this project has been to produce a functional model of an electromagnetic lens system similar to the one found in an Arcam EBM machine. The simulations have been performed using the COMSOL Multiphysics® software and the calculations have been based on the Finite Element Method. Furthermore, additional methods to lower the computational time have been investigated and evaluated. Ultimately the project has aimed to supply GE Additive with insights in how they can build a simulation tool capable of simulating new concepts or alterations to their current EBM lens system and measure their effects on the electron beam.

Explicitly this report will answer the following questions:

- Is it possible to model an EBM like lens system in COMSOL using FEM?
- Is it possible to model an EBM like lens system in COMSOL using BEM?
- How much time is required to compute a FEM simulation?
- How accurate are the calculations within a reasonable time frame?
- What additional methods can be implemented to lower the computation time?
- How reliable are the simulations with the additional implementations?

Throughout this report *evaluation* will be a reappearing term and it is worth clarifying what it means in the context of this project. A simulation model is evaluated to be good if it obtains a good balance between computational time and accuracy, meaning the simulation can be computed in a reasonable time while obtaining sufficiently accurate and reliable results in relation to the computational time. Furthermore, the simulation model should also be sufficiently flexible and simple to use in order to be evaluated as good. Flexibility in this context refers to having a simulation model that can be used to do a wide variety of different tests, e.g. changing the geometry, changing the material properties, implementing heat expansion or introducing external magnetic fields in the model and measuring the effects. Simplicity refers to the tool being easy to use, meaning that it is relatively easy for a majority of the engineers at the company to understand how the tool works and how to use it properly. Note that the evaluation tends to be quite subjective and can only be quantify if the requirements of the simulation tool are explicitly stated.

It should also be noted that certain delimitations have been placed on both the model and the evaluation process to ensure that the project is feasible within the given time and to ensure that the thesis can be published in its entirety without violating immaterial rights towards GE Additive. These delimitations are accounted for in section 3.1.

The structure of the thesis is as follows. After this introduction, the Arcam EBM technology and the necessary theoretical background is presented in Chapter 2. In Chapter 3 the methodology of building the model and simulating the system of

interest is described. In Chapter 4, the results from the simulations are presented. In Chapter 5, recommendations are provided and conclusions are drawn.

1.3 Ethical, Societal and Environmental concerns

Additive Manufacturing is a growing industry with the potential to completely change production processes. Due to the additive nature of AM it has the potential to consume less resources, thereby being more environmentally friendly than traditional methods. However, as the industry is still fairly young, this might not yet be true in practice when evaluating the entire supply chain. Aside from lowering consumption, AM also opens an entirely new field of manufacturing, capable of manufacturing extremely complex geometries. For example medical companies are today able to print customized prosthetic devices such as hip cups or spinal implants in a faster and more accurate way than ever before. Another interesting field is the aerospace industry which uses AM to build lightweight structural components and high performance rotor blades, which help lower the fuel cost and efficiency of the planes. Additionally, the ability of printing complicating geometries can potentially have a large economic impact. By enabling certain parts of a larger structure to be built as one unit instead of separate units the cost of manufacturing and assembling can be lowered as well as the cost of transportation and logistics by shortening the supply chain. It is hard to say exactly what impact AM will have on our society for the foreseeable future, but it is hard to imagine it not having a positive impact regarding technological advancement, sustainability and the development of health care.

The downside with absolute freedom of design is the potential of it being used for terrorism or war. If anything can be designed and built in an AM machine, then that includes devices used in guns and explosives. Objects like these obviously need to be thoroughly regulated and therefore companies like GE Additive have to take responsibility in the matter.

2

Theory

The purpose of this project is to use the COMSOL's FEM solver to simulate the electronic beam in a Arcam EBM. In this chapter the Arcam EBM technology is introduced. The theory and practical arrangements related to electron beam, electron optics and magnetic lens are discussed. Thereafter features of the numerical solver are explained.

2.1 Arcam EBM Technology

Additive Manufacturing (AM) is the general term used for manufacturing methods that manufacture additively, differentiating them from traditional manufacturing methods where the manufacturing is done subtractively. The method of interest, which this project aims to partially simulate, is called Arcam Electron Beam Manufacturing (EBM). Here is a brief explanation of EBM technology for readers unfamiliar with it.

A schematic setup of EBM can be seen in Figure 2.1. The setup can be divided into two parts: the upper Electron Beam Column and the lower Build Chamber. Inside the Column we find the electron source and the magnetic lens system. The electron source is made out of either a tungsten filament or a LaB_6 crystal which emits electrons. The electrons are accelerated into the lens system consisting of five lenses: one focusing lens, two astigmatism lenses and two deflection lenses. The lenses regulate the shape, size and direction of the beam, focusing it on a desired part of the powder surface. The powder is found inside the build chamber which is held at vacuum pressure. This ensures that the electron beam does not interact with the air particles before hitting the

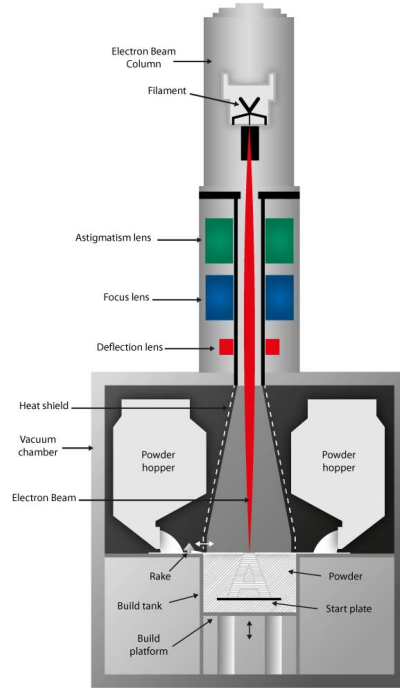


Figure 2.1: Schematic of the entire Arcam EBM machine.

powder. The powder is stored inside the two powder hoppers and using a mechanical rake the powder is deposited onto the build platform. EBM is a layer-by-layer technique. To build a layer the machine first deposits a very thin and even layer of powder onto the build platform. Thereafter it selectively melts certain areas of the powder using the electron beam, before lowering the build platform just enough to make room for the next layer. A thick and heavy stainless steel start plate is used to ensure that the first layers are even. The construction of an EBM object involves several aspects, e.g. geometrical complexity, design software, heat gradients, powder quality and machine maintenance. These topics are outside the scope of this project and will not be discussed. Also not a part of the scope is the electron source and the electron powder interaction, but since they are very closely related to the lens system they will be briefly explained.

2.1.1 Electron Source

The electrons are emitted using a triode electron emitter with a LaB_6 -crystal as cathode. The cathode is placed at the top of the beam column and emits electrons downwards. The crystal is heated to about 2000 K to increase the energy of the electrons and an electrical potential accelerates the electrons out of the crystal. The potential is placed between the crystal (cathode) and a grid cup (anode). The electrical potential on the hot cathode is set to be about -1200 V and the grid cup is grounded. An intermediate grid is placed between the cathode and anode with a separate potential, thereof the name triode emitter. This potential of the intermediate grid can be varied, which allows the user to vary the potential barrier of the electrons, thereby regulating the intensity of the electron beam.

In this project the electron source will be provided as an input parameter produced by previous calculations of the electron source in the CPO software. The specifications of the emission can be found in Appendix A.

2.1.2 Electron-Powder Interaction

The electron-powder interaction heats the metal powder, which can either fully melt it or partially melt (sinter) it. Fully melted powder results in the strongest bond, which is desired when building the actual components. Sintering the powder results in a more porous structure, which is preferable when building support structures. It is therefore important to have complete control over the size and intensity, or more specifically the charge distribution, of the electron beam. It is worth noting that the metal powder must be grounded. Otherwise the electrons will charge the powder to a degree where the metal powder may start causing small explosions due to the negative repulsion.

There are various methods for additive manufacturing in metal on the market today. EBM is often compared to similar methods that use a laser instead of an electron beam and it is worth noting a couple of examples on how they interact differently with the metal powder. The key feature of 3D-printing is the resolution, i.e. the

smallest size possible to distinguish. Here electron beams have a fundamental advantage towards laser beams since the wavelength of an electron can roughly be as low as 5 pm, while visible light has a wavelength of 400 nm to 700 nm. Another way electron beams differ in relation to laser beams is their penetration depth. The mean free path of an electron in a metal medium is about 3-4 orders of magnitude smaller than that of light, which gives EBM a more concentrated depth of heating. Lastly the electron beam is quicker and easier to control due to the flexibility using magnetic fields created by currents, while a laser needs advanced mechanical systems of mirrors to deflect the laser beam.

2.2 Electron Optics

Charged Particle Optics is used to calculate the trajectories of charged particles in electromagnetic fields. In Electron Optics, the electron is the only charged particle of interest, which is characterized by its mass $m_e = 9.109\,383 \times 10^{-31}$ kg and charge $q_e = -1.602\,177 \times 10^{-19}$ C. As a charged particle, the electron will obey the Lorentz Force, see equation (2.1). The equation states that the force exerted on a particle depends on the charge q_e and the velocity \mathbf{v} of the particle as well as the magnetic flux \mathbf{B} and electric field strength \mathbf{E} . The electrons exit the grid cup with an average speed of 1.45×10^8 m/s, about half the speed of light $c = 299\,792\,458$ m/s. This means that relativistic mechanics are required, in which the acceleration of the electron depends on the Lorentz factor $\gamma(\mathbf{v})$, see equation (2.2), where \mathbf{a}_{\parallel} is the acceleration parallel to the velocity and \mathbf{a}_{\perp} the perpendicular. An important thing to note about the Lorentz-equation is that the magnetic force is always perpendicular to the direction of motion. Therefore the magnetic part of the Lorentz force will exert no work onto the electron, meaning that the energy of the electron is conserved in a magnetic field.

$$\mathbf{F} = q_e (\mathbf{v} \times \mathbf{B} + \mathbf{E}) \quad (2.1)$$

$$\mathbf{F} = \frac{d}{dt} (\gamma(\mathbf{v}) m_e \mathbf{v}) = \gamma(\mathbf{v})^3 m_e \mathbf{a}_{\parallel} + \gamma(\mathbf{v}) m_e \mathbf{a}_{\perp} \quad (2.2)$$

$$\gamma(\mathbf{v}) = \frac{1}{\sqrt{1 - \frac{\mathbf{v}^2}{c^2}}} \quad (2.3)$$

2.2.1 Beam Properties

A group of electrons traveling collectively is called an electron beam. By defining certain properties of the beam it can help characterize how the beam will interact with the powder when it reaches the powder surface. Mainly, it is of interest to know what area of powder will be melted and with what intensity. The two main properties are therefore Hyperemittance, which describes the spatial distribution, and Brightness, which describes the charge density distribution. These two quantities are highly correlated, in the sense that a low hyperemittance results in a high

brightness and vice versa. This can be related to the powder interaction, where a high brightness results in fully melted powder and a low brightness results in sintered powder.

A 10 mA electron beam creates a flow of about 6.2×10^{16} electrons per second. It is not feasible to model that many particles. Instead only a thousand or so electrons are modeled to interact with the magnetic coils and their individual contributions are scaled accordingly.

From the electron position (x, y, z) and the electrons momentum (p_x, p_y, p_z) , an electron will have six degrees of freedom $\{x, p_x, y, p_y, z, E\}$, where z is chosen to be the principle direction of the electron beam and p_z is substituted with the electron energy E by convention. E can often be viewed as constant, due to the energy conservation of the magnetic Lorentz force. For any value of z a cross-section can be defined with four degrees of freedom $\{x, p_x, y, p_y\}$. The area covered by the projection of the particles positions $\{x, y\}$ in a cross-section defines the hyperemittance. The brightness of the cross-section is in this project defined as the probability density function obtained from placing a normal distribution at each point $\{x, y\}$. Another useful property is the emittance ϵ , defined by the area $A = 4\pi\epsilon$ of the phase-space projection of the parameters $\{x, x'\}$, where $x' = p_x/p_z$. Hyperemittance, brightness and emittance are visualized in Figure 2.2. [3]

The root-mean-square of the emittance can be quantified using equation (2.4). The area of the phase-space projection is thereafter approximated as $A = 4\pi\epsilon_{1-rms}$. Afterwards the Twiss parameters (α, β, γ) are introduced, see equation (2.5). γ and β are proportional to the elongation in the x' -direction and the x -direction respectively. They are also inversely proportional to each other. α is proportional to the angle of the tilt. An upright ellipse corresponds to $\alpha = 0$. The beam is converging for $\alpha > 0$ and diverging for $\alpha < 0$. [3]

$$\epsilon_{1-rms} = \sqrt{\langle x^2 \rangle \langle x'^2 \rangle - \langle xx' \rangle} \quad (2.4)$$

$$\gamma = \frac{\langle x'^2 \rangle}{\epsilon_{1-rms}} \quad \beta = \frac{\langle x^2 \rangle}{\epsilon_{1-rms}} \quad \alpha = \frac{\langle xx' \rangle}{\epsilon_{1-rms}} \quad (2.5)$$

A simple way to define the focal plane is to find the value of z where $\alpha = 0$, see the converged emittance in Figure 2.2. The brightness can then be used to obtain the diameter of the focal point, also called the spot size. The diameter of the spot is defined as the Full Width Half Max (FWHM) of the electron charge distribution. By assuming that the charge has a Gaussian distribution ($f(x) = A \exp(-x^2/2\sigma^2)$) the FWHM can be calculated as $\text{FWHM} = 2\sqrt{2 \ln 2} \sigma$ of the hyperemittance. The relationship is easily proven by finding the values x for which $f(x) = A/2$. Since the data is two-dimensional, different directions can have different standard deviations and therefore different spot sizes. Using Principle Component Analysis (PCA) the

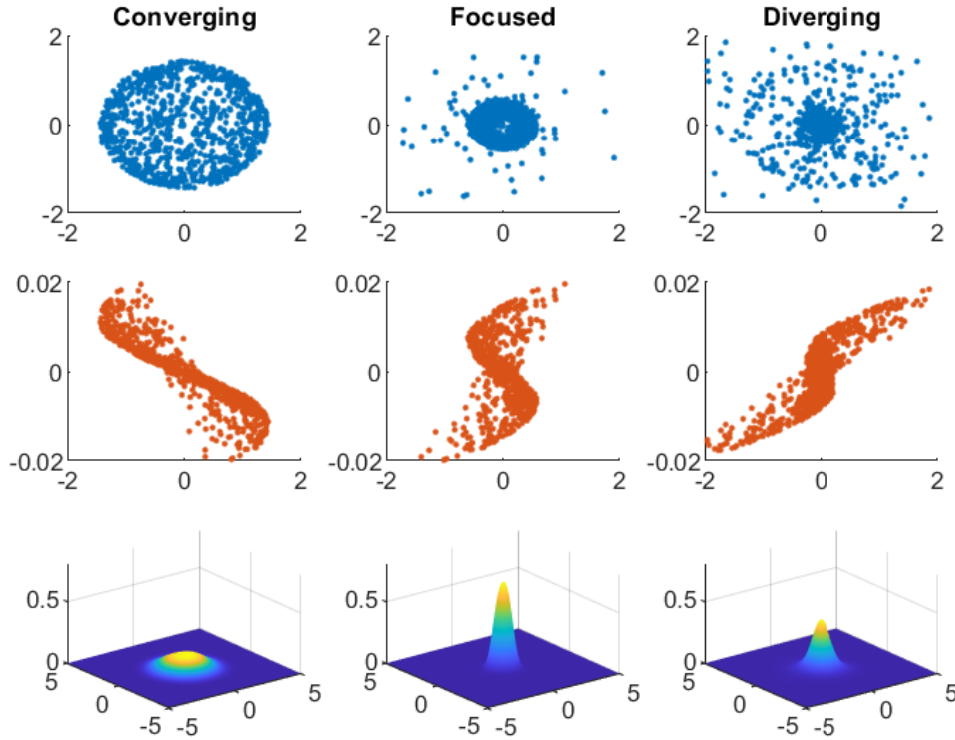


Figure 2.2: Hyperemittance (top), Emittance (middle) and Brightness (bottom) for the cross-section of a beam when it is Converging, Focused and Diverging.

principal direction with the largest standard deviation $\sigma_{\parallel\text{PCA}}$ can be found. Comparing $\sigma_{\parallel\text{PCA}}$ to the standard deviation of the orthogonal direction $\sigma_{\perp\text{PCA}}$ gives an estimation of the astigmatism of the focal point.

2.2.2 Electron-electron interaction

Aside from the external interaction with the magnetic coils the electrons also interact amongst themselves. The electron-electron interaction is due to the electrical force from the Coulomb repulsion as well as the magnetic force created from their own movement. In this study the electrical force is taken into consideration, especially in the vicinity of the focal point where the electron density is the highest, but the magnetic force is neglected. The magnetic force can be neglected because it is only a fraction of the size of the electric force. To estimate the electric and magnetic force on a electron a system of two parallel currents can be set up and evaluated, see Figure 2.3. Two infinitely long currents I running parallel at a distance r from each other. They contain n electrons per unit length and therefore they have a charge nq_e per unit length. The electrons travel at about half the speed of light $v \approx c/2$, for which we can express the current as $I = nq_ev$. The currents produce an electrical field $E_r = q_en/2\pi\epsilon_0r$ (derived from Gauss's flux theorem $\nabla \times \mathbf{D} = \rho$) and a magnetic field $B_r = \mu_0nev/2\pi r$ (derived from Ampere's law $\nabla \times \mathbf{H} = \mathbf{J}$). The electric force per unit length F_E and the magnetic force F_M per unit length can

from this be expressed, as seen in equations (2.6) and (2.7).

$$F_E = q\mathbf{E} = q_enE_r = \frac{q_e^2n^2}{2\pi\epsilon_0} \frac{1}{r} \quad (2.6)$$

$$F_B = q(\mathbf{v} \times \mathbf{B}) = q_envB_r = \frac{\mu_0(nqv)^2}{2\pi} \frac{1}{r} \quad (2.7)$$

$$F_E - F_B = \frac{q_e^2n^2}{2\pi\epsilon_0} (1 - \epsilon_0\mu_0v^2) \frac{1}{r} = \frac{q_e^2n^2}{2\pi\epsilon_0} \left(1 - \frac{v^2}{c^2}\right) \frac{1}{r} = \frac{q_e^2n^2}{2\pi\epsilon_0} \gamma(v)^{-2} \frac{1}{r} \approx \frac{3}{4} F_E \quad (2.8)$$

When comparing the electric force F_E and the magnetic force F_B per unit length, see equation (2.8), it is found that $F_B = (1 - \gamma^{-2})F_E$, meaning they only differ by a factor $1 - \gamma(v = c/2)^{-2} \approx 1/4$. For a physicist interested in relativity, it becomes quite fascinating that the magnetic force cancels the electric force. The contribution from the magnetic field is actually equivalent to a reduced charge density in the currents. This is a consequence of the Lorentz elongation $L = L_0\gamma(v)$ of the distance between the electrons in the current when changing the frame of observation from a stationary frame to a frame moving with the electrons at a speed of v . Because, when moving with the electrons, the electrons are stationary and therefore there will be no current to produce a magnetic field. A rather counterintuitive consequence of this is that the forces will cancel each other out for electrons moving at speeds close to the speed of light, meaning both forces can be neglected. With the electrons moving at about half the speed of light, the magnetic force will be approximately a quarter of the electric force. Arguably, a 25% difference could be a contribution worth including, but in this study it has been chosen to be neglected all the same. This is partly motivated because the magnetic field was neglected when producing the electron source data, meaning the trajectories already have a proportional error on the angular distribution.

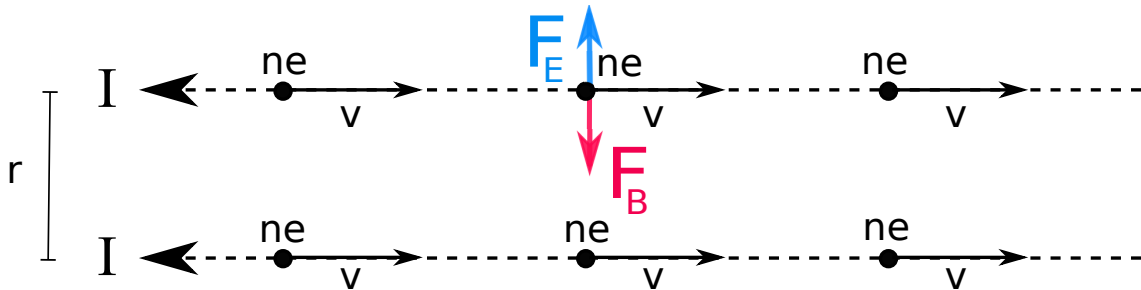


Figure 2.3: The electron-electron interaction between two infinite parallel currents $I = nqv$ a distance r apart. For $v = c/2$ the magnetic force per unit length F_B can be found to be a quarter of the electric force per unit length F_E .

2.3 Magnetic fields and Magnetic Lens Design

The lens system is made out of five lenses: a focusing lens, two deflection lenses and two astigmatism lenses. This section will in detail explain what magnetic fields they

produce and how the fields effects the electrons.

A magnetic fields is created by running a current \mathbf{I} through a wire. The relationship between the magnetic fields and the current is described by Ampere's law (2.9), one of Maxwell's laws of electromagnetics. The law states that the curl of the magnetic field strength \mathbf{H} equals the current density \mathbf{J} plus the time derivative of the electric displacement field \mathbf{D} . For static currents the time derivative becomes zero. When simulating in a vacuum environment the magnetization \mathbf{M} and polarity \mathbf{P} are also zero. The magnetic lenses in this project consist of two basic building blocks: straight wires and circular wires. The resulting magnetic field created by running a current through a straight wire and a circular wire are found in figure 2.4. More complicated lens designs will be discussed later on in the text and it can be helpful to break it down into these basic structures. For simplicity all magnetic fields in this project are calculated for a perfect vacuum with permittivity ϵ_0 and permeability μ_0 , see equation 2.11, whose values are directly related to the speed of light c_0 , see equation 2.12. In reality ferromagnetic materials such as iron are used to control the magnetic flux density.

$$\nabla \times \mathbf{H} = \mathbf{J} + \frac{\partial \mathbf{D}}{\partial t} \quad (2.9)$$

$$\mathbf{H} = \frac{\mathbf{B}}{\mu} - \mathbf{M} \quad \mathbf{D} = \epsilon \mathbf{E} + \mathbf{P} \quad (2.10)$$

$$\epsilon_0 = 8.854 \times 10^{-12} \text{As/Vm} \quad \mu_0 = 4\pi \times 10^{-7} \text{Vs/Am} \quad (2.11)$$

$$c_0 = \frac{1}{\sqrt{\epsilon_0 \mu_0}} = 2.998 \times 10^8 \text{m/s} \quad (2.12)$$

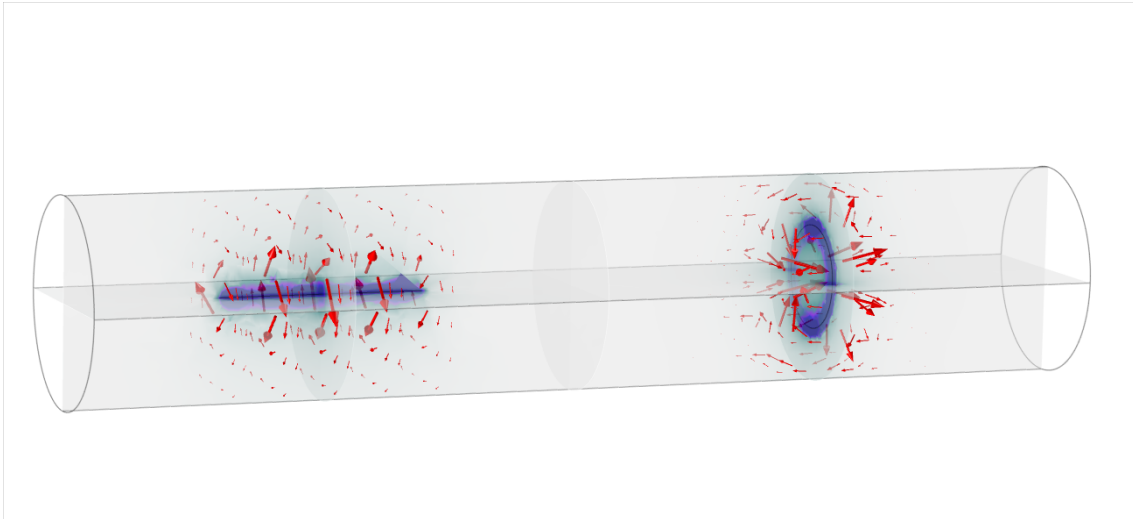


Figure 2.4: The magnetic fields created by a straight wire and a circular wire. The darker color indicates a stronger magnetic field strength and the arrows indicate the direction of the field.

2.3.1 The Focus Lens

The Focus Lens is the most important and the most powerful of the five lenses. By focusing the electron beam onto the powder surface a smaller area is hit with a higher density of electrons. And the other way around, by defocusing the electron beam, a larger area is hit with a lower density of electrons. Both options are important for different applications, whether it is desired to simply sinter or fully melt the metal powder. Having complete control over the focal length, and thereby the spot size, is key to successfully building objects with high resolution.

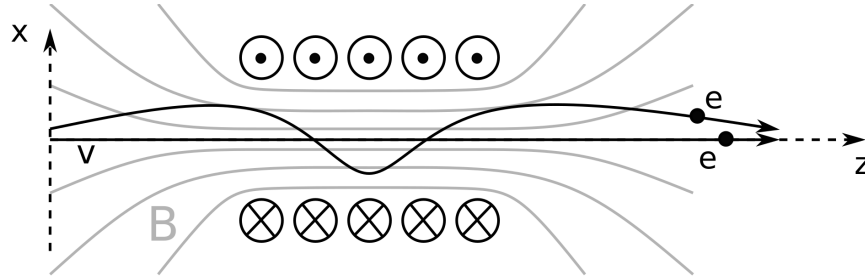


Figure 2.5: A schematic of the magnetic field B created by a solenoidal with five turns and how electrons with and without initial angles interact with it. The wavy trajectory of the angled electron represents the spiraling effect associated with the convergence.

The design of a focus coil is fairly simple, but the focusing phenomenon is not trivial. The design is a simple solenoidal coil, a spiral of circular coils. The magnetic field strength mainly depends on the current that passes through the coil, the number of turns and the length of the coil. A schematic figure of a focus coil with five turns can be found in Figure 2.5. The magnetic flux density \vec{B} mainly points in the positive z -direction and is fairly homogeneous inside the coil, i.e. $\vec{B} \approx B_z$. Outside the coil the field becomes weaker and loses its homogeneity. The figure has two electrons interacting with the field. The first electron has a velocity $\vec{v} = v_z$ and travels along the optical axis. The electron only experiences a magnetic field parallel to itself, meaning the magnetic force is zero. This is due to the cross-product in the Lorentz force, i.e. $v_z \times B_z = 0$. The second electron approaches the coil at a slight angle, which means that it has a radial velocity v_r entering the coil. The angle allows interaction with B_z , resulting in an azimuthal force $q(v_r \times B_z) = F_\phi$. The azimuthal force forces the electron to start spiraling. The spiraling motion means that the electron now has a azimuthal velocity v_ϕ which creates a negative radial force, i.e. $q(v_\phi \times B_z) = -F_r$. This forces the electron towards the optical axis, thereby focusing the electron. The larger the initial angle, the larger the converging force becomes, which forces all the electrons to meet in the focal point. The position of the focal point on the z -axis is called the focal length f and a thin lens approximation can be made to roughly estimate its value, see equation (2.13). An ideal focus lens will create an image of the electron source in the focal plane. If the source is a point, the image will be a point. A real focus lens is however flawed and non-ideal aberrations are introduced as the electrons propagate through it. Two basic aberrations

are spherical and chromatic aberrations. Spherical aberrations are when electrons located at different radial positions interact differently with the lens. Commonly the magnetic field within the focus coil will not be completely homogeneous and electrons propagating further from the optical axis will experience a different focusing effect. Chromatic aberrations occur when there exists an energy distribution among the electrons. The focusing effect depends on the velocity, and if the electrons have different energies, they will have different velocities.

$$\frac{1}{f} = \frac{e^2}{8m_e E_0} \int B_z^2 dz \quad (2.13)$$

When working with a EBM machine it is often preferable to not focus the electron beam directly on the powder surface. Instead the focus point is chosen to be a couple millimeters before the powder surface. This distance is called the offset and it helps to produce a more stable spot size. The electrons will experience a high electrical potential in the focal point, which will smear out the electron distribution. If the crystal is slightly chipped or cracks during a build, the focus offset will help to smear out whatever effects occur because of this.

2.3.2 The Deflection Lens

When building 3D objects it is useful to utilize the entire build surface. The Focus Lens is only capable of focusing the beam onto the optical axis and therefore a second type of lens is required to deflect the beam. The deflection lens does this by creating a homogeneous magnetic field perpendicular to the optical axis. Ideally a perfect homogeneous magnetic field B is set up within a confined space with a length d , as seen in Figure 2.6. Then the angle of deflection φ can be found to be proportional to B for small angles, see equation (2.14). By altering the strength and the direction of magnetic field it is therefore possible to focus the beam onto the entire surface. To compensate for the increased distance the remaining focal length will be multiplied by a factor $\cos^{-1} \varphi$ and the current of the Focus Lens should be corrected accordingly.

$$\varphi = \arcsin \frac{q_e B d}{m_e v} \approx \frac{q_e B d}{m_e v} + \frac{1}{6} \left(\frac{q_e B d}{m_e v} \right)^3 + \mathcal{O} \left(\frac{q_e B d^5}{m_e v} \right) \quad (2.14)$$

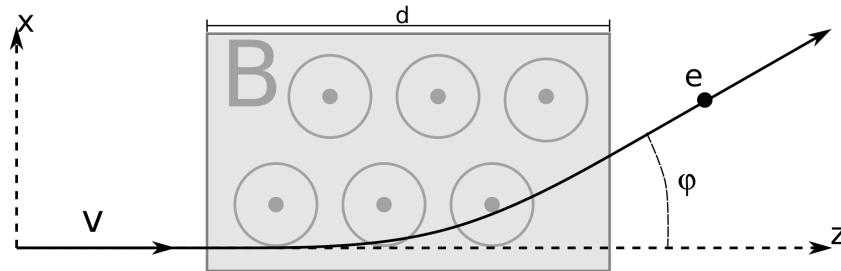


Figure 2.6: Deflection of an electron in a homogeneous magnetic field.

Ideally the deflection lens creates a perfect homogeneous field, but realistically it can only approximate it. However, with the right design the approximation comes rather close. The design of the Deflection Lens is fairly complex and therefore four of models with increasing complexity are presented in Figure 2.7 to show where the design originates. The first and most simple coil is found to the far left. It is called the Helmholtz coil and consists of two single circular coils with equidirectional currents. Both circular coils create a homogeneous field through the center of their circles, and therefore a somewhat homogeneous field is created between them. The homogeneity is increased in the second lens by adding two additional circular coils at specific positions. The lens is called a modified Maxwell coil (the true Maxwell coil only has three circular coils). In the third model the circular wires are replaced with squares. This does not significantly change the magnetic field, but it helps show the transition to the final coil: the Saddle Coil. In this coil the top and bottom wires of the squares are replaced by circle segments, forming saddle shaped wire segments. The lens design can also be referred to as an air-coil with semi-distributed winding [4]. Aside from increasing the homogeneity, the design also opens up a larger area for the electrons to travel through without hitting the coil. The number of vertical wires in the Saddle Coil denotes the coils order.

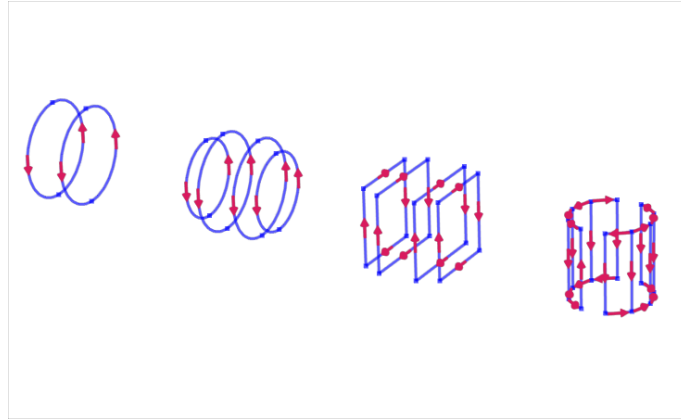


Figure 2.7: Four models of deflection lenses of increasing complexity. From left to right: a Helmholtz coil, a modified Maxwell coil, a square modified Maxwell coil and a Saddle Coil. All coils approximate a homogeneous magnetic field.

The actual Saddle Coil used in the EBM machine is of the 24th order, see Figure 2.8. It is worth noting that the wires must be physically accurate, meaning no current can abruptly end by itself. Otherwise Kirschoff's circuit law is broken and it would be impossible to physically build the coil. The vertical wires are indexed with numbers $i = 1, 2, 3, \dots, 24$ and placed at an angle $\theta_i = i\pi/12 - \pi/24$ on the perimeter of the cylinder. It can be analytically derived that the homogeneity is maximized when currents have a sinusoidal distribution [5]. Therefore, to create a homogeneous field in the x-direction, the currents of each wire are expressed as $I_i = I_x \sin \theta_i$, where a positive current represents a current in the positive z-direction. To create a magnetic field in the y-direction the phase of the currents are shifted 90 degrees (the angle between the x-direction and the y-direction) and the expression instead becomes $I_i = I_y \cos \theta_i$. With two independent deflection coils their magnetic fields can be

super-positioned to create a homogeneous field in any direction in the xy-plane. In practice this requires two separate sets of wiring in order to control the currents individually, but when modeling the coil it is sufficient to simply superposition the currents, see equation (2.15).

The vertical wires are then joined by the circle segments as seen in Figure 2.8. To explicitly state their currents the circle segments will be defined as short arcs, covering an angle $\pi/12$, placed between two neighbouring vertical wires. They are indexed with numbers $j = \pm 1, \pm 2, \pm 3, \dots, \pm 24$ and placed at angles $\phi_j = (|j| - 1)\pi/12$ either on the top (+) or the bottom (-) of the cylinder. The current passing through an arc is the sum of the contributions from several vertical wires and it also has a sinusoidal distribution, but the distribution will be phase-shifted 90 degrees (much like how the integral of the sine function is a cosine function). It can be expressed as in equation (2.15), where the prefactor $N = \sum_{i=1}^6 \sin \theta_i$ ensures that Kirschhoff's law is fulfilled. A positive current in this case represents a clock-wise direction. As a final note, when building the model practically, the terms $\sin \theta_i$, $\cos \theta_i$, $\sin \phi_j$ and $\cos \phi_j$ must be rounded to the closest integer value, since it is impossible to wire a decimal number of revolutions.

$$I_i = I_x \sin \theta_i + I_y \cos \theta_i \quad I_j = \text{sgn}(j)N [I_x \cos \phi_j + I_y \sin \phi_j] \quad (2.15)$$

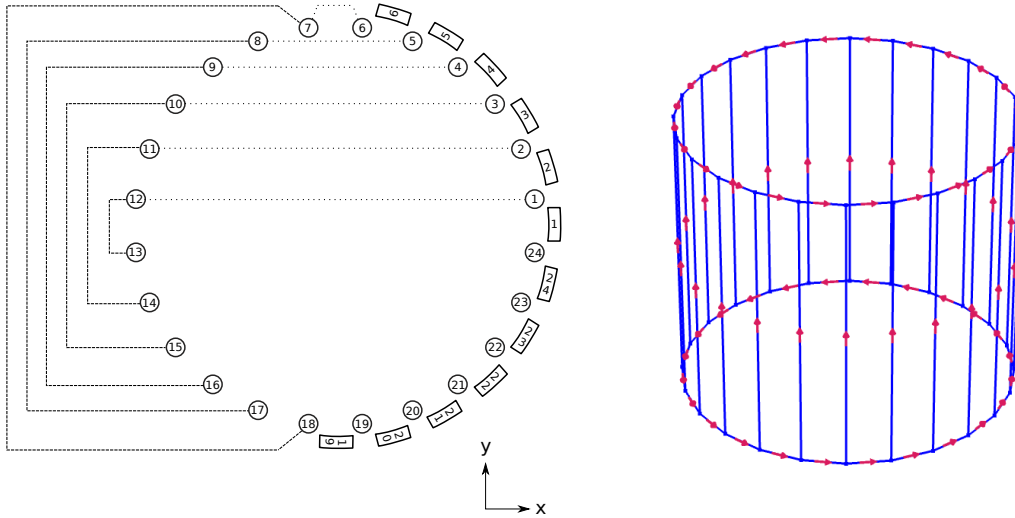


Figure 2.8: The design and layout of a 24th order Saddle Coil. The left schematic displays a top view of the coil and how the vertical wires (circles) and circle segments (arcs) are indexed. The dashed lines show which vertical wires are directly connected when creating a magnetic field in the x-direction and the dotted for the y-direction. The right figure shows a 3-dimensional view of the deflection coil in COMSOL.

2.3.3 The Astigmatism Lens

The concept of astigmatism is an aberration that relates to a non-circular shape of the beam in a cross-section. The term astigmatism is often associated to an elliptical shape of the hyperemittance. However, in general there are multiple folds of

astigmatism describing more complex aberrations. This section will limit itself to only discuss elliptical 2-fold astigmatism and exclude higher orders of astigmatism.

To counter the elliptical feature a magnetic field is desired which elongates the beam on its short axis and pushes it together on its long axis. This can be achieved with a quadrupole lens with alternating polarity, also called a stigmator, see Figure 2.9. The elliptical features can be removed on the x- and y-axis by adjusting the directions and amplitudes of the currents in the coils. To be able to remove elliptical features in all directions a superposition of two stigmators are required, positioned at an angle $\pi/4$ relative each other.

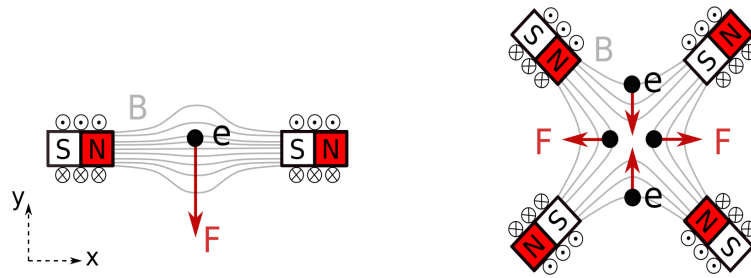


Figure 2.9: Deflection lens (left) and astigmatism lens (right).

From Figure 2.9 it can be seen that the astigmatism lens design is quite similar to the deflection lens. The deflection design has two poles in series and the astigmatism has four alternating poles. It becomes apparent that an astigmatism lens can be created from two deflection lens with inverted currents on one of the sides, as has been done in equations (2.16) and (2.17). This means that there is essentially no difference computationally between a deflection lens and an astigmatism lens.

$$I_i = \text{sgn}(\cos \theta_i) I_x \sin \theta_i + \text{sgn}(\sin \theta_i) I_y \cos \theta_i \quad (2.16)$$

$$I_j = \text{sgn}(j) N [\text{sgn}(\cos \phi_j) I_x \cos \phi_j + \text{sgn}(\sin \phi_j) I_y \sin \phi_j] \quad (2.17)$$

2.4 Numerical Methods

Given a problem defined by a set of equations, if the solution can not be calculated analytically, a numerical method can be used to find an approximate solution. The difference between the exact solution and the approximate is called the error. The goal of all numerical methods is to be able to minimize the error to an arbitrary level. This ensures that the solution converges to the exact solution. The error is decreased by increasing the resolution. For this project the resolution will refer to the number of elements used to divide a volume or surface in the FEM method and the time step in the time stepping algorithms.

2.4.1 Finite Element Method

The Finite Element Method is a highly established numerical method used in many fields such as computational fluid dynamics and mechanics of materials. The key strength of FEM compared to other numerical methods is its ability to deal with complex geometries. This section will briefly introduce the mathematical theory behind FEM before discussing how to control and optimize the mesh.

The general recipe for the method starts by subdividing the domain into cells, also called meshing. Cells inside the volume are 3-dimensional and cells on the surface are 2-dimensional. Commonly the volume cells have a pyramid or tetrahedral geometry and the surface cells have a triangular geometry. The cells are defined by the position of their nodes (corner points). A triangle has three nodes, a tetrahedron four and a pyramid five. For each node a nodal basis function is defined that is non-zero within the volume of the neighbouring cells and zero outside them. The function value is calculated in the node and decays linearly to zero towards the outer surface of the neighbouring cells. Together the nodal functions create a complete set of linearly independent basis functions that span the entire volume of the meshed object. The function value of any point within the meshed volume can thereafter be approximated as a linear combination of the nodal basis functions. Note that only the nodal functions of the nodes to the cell which the points lies within contribute to function value. The weights of the linear combination are found by minimizing some explicitly stated error. A simple illustration of FEM for a 1-dimensional domain can be seen in Figure 2.10.

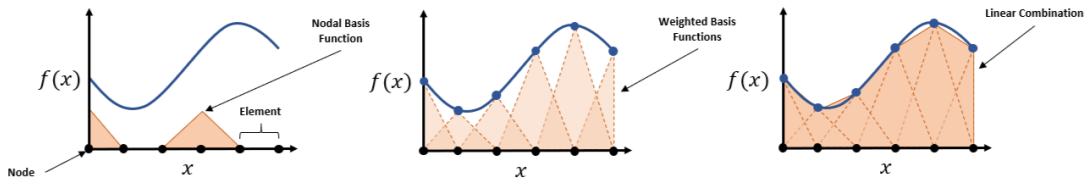


Figure 2.10: A simplified illustration of how a target function $f(x)$ can be numerically approximated on a 1-dimensional domain x .

The general problem can be set up mathematically as $L[f] = s$, where the operator L describes the physics and the source s describes the conditions of the system. The target function f is unknown and sought to be found for all points in the domain Ω . When calculating a magnetic field the entire expression $L[f] = s$ would boil down to Maxwell's equations, where f would represent the magnetic vector potential \mathbf{A} . The magnetic vector potential is related to the magnetic flux density as $\mathbf{B} = \nabla \times \mathbf{A}$. The source s would then represent the current density and charge density of the system. The approximate solution to f is thereafter defined as a linear or quadratic combination of the nodal basis functions φ_i and their respective weights f_i , see equation (2.18). The nodal basis functions are visualized in Figure 2.10. [6]

$$f(r) = \sum_{i=1}^n f_i \varphi_i(r) \quad (2.18)$$

The system is said to converge when the residual $r = L[f] - s$ approaches zero everywhere. This condition can be a little hard to fulfill and is therefore commonly relaxed by requiring that only the average weighted residual must equal zero. In other words, this is not a point-wise convergence. To calculate the average residual a test functions w_i is introduced. In general Galerkin's method is used, where the test functions is defined to be equal to the nodal basis function, $w_i = \varphi_i$. The weighted residual is then computed as:

$$\langle w_i, r \rangle = \int_{\Omega} w_i r d\Omega = 0 \quad (2.19)$$

This equation becomes a series of linear equations depending on f_i . To solve the system of equations, appropriate boundary conditions must be introduced. Once solved, the weights f_i are put into equation 2.18 and the function value can be approximated for all points in Ω . [6]

2.4.1.1 Mesh optimization

With the general mathematical theory established, the focus can be shifted towards how FEM can be used as a computational tool in practice. In general, what determines the quality of the simulation, is the resolution of the spatial mesh. Too few elements will give a larger error in the magnetic field calculations, while too many mesh elements will consume an unnecessary amount of computational time. The art of the craft is to be able to place an appropriate amount of elements. In general this means seeking a higher element density in regions where the magnetic field changes a lot.

COMSOL offers five basic variables allowing the user to control the mesh of a domain. Maximum element size ($hmax$) and minimum element size ($hmin$) control the size of the elements, where the element size is defined as the longest straight line within the element. The growth rate ($hgrowth$) defines the maximum size ratio between two neighbouring cells. FEM finds it harder to resolve arches than lines, because of the basic geometry of the elements. The curvature factor ($hcurve$) helps resolve curved geometries by increasing the number of elements in these regions. Similarly the resolution of narrow regions factor ($hnarrow$) increases the resolution of narrow regions.

The COMSOL meshing algorithm is as any other licensed software somewhat of a black box, but it can be explained in broad terms. The algorithm starts with the geometrical layout defined by the user. For a simple cube this consists of a volume, defined by six square surfaces, which in turn are defined by the twelve edges, defined by the eight nodes of the cube. The algorithm starts from the lowest dimension, meshing the edges first, the surfaces thereafter and the volume last. When meshing, the algorithm iteratively introduces nodes into the domain, which defines new cells, and thereafter controls that all new elements fulfill the criteria determined by

the predefined variables h_{\max} , h_{\min} , h_{growth} , h_{curve} and h_{narrow} . If an element violates a criterion, new nodes are once again introduced within the domain of the element, breaking it up into smaller cells. This process solves the violations of all basic criteria except h_{\min} . The minimum element size criterion is harder to correct when violated as it requires the removal of nodes. In general, the mesh algorithm seems to ignore correcting h_{\min} violations and settle with throwing an error message. The meshing algorithm implemented by COMSOL is deterministic, meaning the same mesh structure is always achieved for the same geometry with the same meshing parameters. In other words there is no randomness involved when the algorithm chooses to insert new node.

All throughout the meshing algorithm, the COMSOL software seeks to maximize the element quality. The quality can be defined in a number of different ways. The general idea of a high quality element is that it has an ideal geometry with a large volume to surface ratio. A computational demand of an element is mainly determined by the number of nodes, and therefore it is computationally beneficial to divide the domain into fewer elements with larger volume than vice versa. Another important aspect when obtaining a high quality mesh is to minimize the distance between the points in the volume to their closest node. Because the field value is calculate in the nodes, the best approximations are found in the close vicinity. The most common measurement of quality is the skewness, a dimensionless number between 0 and 1, defined by equation (2.20), where θ is an angle taken over a vertice or edge on the element E and θ_e is the angle of the ideal geometric shape. A completely flat element will have a skewness of 0, while an ideal element will have a skewness of 1. Several other definitions of quality exist that may be more beneficial in certain circumstances.

$$\text{Skewness}_E = \min_{\forall \theta \in E} \left[1 - \max \left[\frac{\theta - \theta_e}{180 - \theta_e}, \frac{\theta_e - \theta}{\theta_e} \right] \right] \quad (2.20)$$

The meshing parameters enable the user to resolve the system arbitrarily fine. The question that follows becomes how to identify when the system is resolved sufficiently fine. This is done by looking at convergence. For a series of systems with increasing resolution, convergence is achieved when the results of the systems remains the same despite increasing the resolution. The series of systems is called a series of iterations and the result of each iteration is defined by some convergence variable. In this study three convergence variables are investigated: magnetic energy E_B , average positional displacement Δr and full width half max FWHM. The magnetic energy E_B is calculated by integrating the energy density of the nodes n of the system, see equation (2.21), where $n \in \Omega$ denotes all the nodes within the domain and $V(n)$ is the volume associated with the node. This method of evaluating the mesh convergence is highly dependant on the number of elements within the foil region, where the magnetic field is strongest. The downside of this method is its inability to determine whether or not the other regions are sufficiently resolved. This is mainly of importance in the focal point, where the electric field strength is relatively high and must be resolved accordingly. The magnetic energy is expected to decrease with each iteration until it converges to a constant value.

$$E_B = \sum_{n \in \Omega} \frac{V(n)}{2\mu_0} \mathbf{B}(n) \cdot \mathbf{B}(n) \quad (2.21)$$

The average positional displacement Δr quantifies the difference in position of the trajectories in the focal plane between iterations, see equation (2.22), where N is the number of particles and $\mathbf{r}_{i,j}$ is the j^{th} particle position in the focal plane for mesh iteration i . The model has converged when $\Delta \bar{r}_i$ approaches zero. Essentially, this method gives the true answer to whether or not the model has converged, since the measurement is the result itself. The downside of this method is obviously the computational cost as it requires not only the computation of the new magnetic field, but also the computation of the electric field and the electron trajectories with each mesh iteration. The $\text{FWHM} = 2\sqrt{2 \ln 2} \sigma$ is calculated from the same data as Δr , but describes the spot size instead of the positional difference. The FWHM is therefore less sensitive than Δr and may converge faster.

$$\Delta \bar{r}_i = \frac{1}{N} \sum_{j=1}^N |\mathbf{r}_{i,j} - \mathbf{r}_{i-1,j}| \quad (2.22)$$

2.4.2 Particle Trajectory Calculations with Time Stepping

The electron trajectory calculations are dependent of time, unlike the stationary magnetostatic field. Events that occur in the beginning of the optical system will impact the rest of the electrons trajectories. Therefore the electrons must be propagate through the entire optical system in order to calculate their positions in the focal plane. Traveling at half the speed of light, the electrons traverse the 1000 mm long beam column within 10 ns. The total elapsed time is discretized into smaller time steps t_i , each for which the trajectory position $\mathbf{r}_i = \{x, y, z\}_{t=t_i}$ and velocity $\mathbf{v}_i = \{v_x, v_y, v_z\}_{t=t_i}$ can be calculate. The position and velocity at a time t_i depends on the previous position and velocity at time t_{i-1} as well as the force $F(\mathbf{r}_{i-1})$ acting on the electron in that position. A very simple time step algorithm is the backwards Euler. Given initial values for \mathbf{r}_0 and \mathbf{v}_0 , the trajectories are then calculated as $\mathbf{r}_{i+1} = \mathbf{r}_i + \mathbf{v}_i \Delta t$ and $\mathbf{v}_{i+1} = \mathbf{v}_i + \mathbf{a}_i \Delta t$, where $F(\mathbf{r}_i) = a_i m_e$ and $\Delta t = t_{i+1} - t_i$.

2.4.2.1 The Generalized Alpha Method

The default transient solver for COMSOL Multiphysics® is the Generalized Alpha method, which is second order accurate (truncation error of order $\mathcal{O}(\Delta t^2)$). This section will discuss the mathematical setup formulated by J. Chung [7]. The strength of the Generalized Alpha method is that it gives the user the ability to chose the degree of high-frequency dissipation by setting the values of the Alpha parameters α_m and α_f . Dissipation means cutting of high frequency movement. Dissipation tends to make the simulation more robust, but it may also reduce the accuracy.

The method was originally developed for structural mechanics and it is intended to describe the positional changes in particle structure due to an external load, thereof the coefficients mass M , damping C and stiffness K . The algorithm determines

the relationship between the external forces \mathbf{F} and the position \mathbf{r} , velocity \mathbf{v} and acceleration \mathbf{a} of the electrons, see equation (2.23).

$$M\mathbf{a}_{i+1-\alpha_f} + C\mathbf{v}_{i+1-\alpha_f} + K\mathbf{r}_{i+1-\alpha_m} = \mathbf{F} \quad (2.23)$$

Equations (2.24) and (2.25) update the displacement and velocity between timesteps. They introduce parameters β and γ which determine the proportion between \mathbf{a}_i and \mathbf{a}_{i+1} . An even proportion is achieved by setting $\gamma = 2\beta = 0.5$. These equations originate from the Newmark method, a predecessor to the Generalized Alpha method. A compact expression $\mathbf{X}_{i+1} = \mathbf{A}\mathbf{X}_i$ can be set up for $\mathbf{X}_i = \{\mathbf{r}_i, \Delta t\mathbf{v}_i, \Delta t^2\mathbf{a}_i\}$. \mathbf{A} is called the amplification matrix.

$$\mathbf{r}_{i+1} = \mathbf{r}_i + \Delta t\mathbf{v}_i + \frac{\Delta t^2}{2} [(1 - 2\beta)\mathbf{a}_i + 2\beta\mathbf{a}_{i+1}] \quad (2.24)$$

$$\mathbf{v}_{i+1} = \mathbf{v}_i + \Delta t [(1 - \gamma)\mathbf{a}_i + \gamma\mathbf{a}_{i+1}] \quad (2.25)$$

In equations (2.26), (2.27) and (2.28) the Alpha parameters are introduced, defining intermediate time steps $\mathbf{t}_{i+1-\alpha_f} = (1 - \alpha_f)\mathbf{t}_{i+1} + \alpha_f\mathbf{t}_i$ and corresponding positions, velocities and accelerations.

$$\mathbf{r}_{i+1-\alpha_f} = (1 - \alpha_f)\mathbf{r}_{i+1} + \alpha_f\mathbf{r}_i \quad (2.26)$$

$$\mathbf{v}_{i+1-\alpha_f} = (1 - \alpha_f)\mathbf{v}_{i+1} + \alpha_f\mathbf{v}_i \quad (2.27)$$

$$\mathbf{a}_{i+1-\alpha_m} = (1 - \alpha_m)\mathbf{a}_{i+1} + \alpha_m\mathbf{a}_i \quad (2.28)$$

The time step algorithm can be shown to be second order accurate. If γ is defined as in equation (2.29), then the first order truncation error can be shown to become zero. The definition of β and the inequality placed on the Alpha parameters ensure that the method is unconditionally stable.

$$\gamma = \frac{1}{2} - \alpha_m + \alpha_f \quad \beta = \frac{1}{4}(1 - \alpha_m + \alpha_f)^2 \quad \alpha_m \leq \alpha_f \leq \frac{1}{2} \quad (2.29)$$

To determine the values of the Alpha parameters the spectral radii $\rho_\infty \in [0, 1]$ is introduced. The spectral radii depends of the eigenvalues to the amplification matrix \mathbf{A} , but for the purpose of this project it is enough to simply state that $\rho_\infty = 1$ represents a no dissipation case and $\rho_\infty = 0$ represents a so-called asymptotic annihilation case, where high frequency responses are annihilated within one time step. The user decides what degree of dissipation is desired and can thereafter calculate the Alpha parameters using equation (2.30).

$$\alpha_m = \frac{2\rho_\infty - 1}{\rho_\infty + 1} \quad \alpha_f = \frac{\rho_\infty}{\rho_\infty + 1} \quad (2.30)$$

It must be noted that the time stepping algorithm used by COMSOL is based on the Generalized Alpha method, but can not be explained in detail by it. Once again the commercial software is somewhat of a black box. An important aspect is how the

time step is chosen. COMSOL uses an algorithm that systematically tries to increase the time step to lower the computational time. With each time step an error value is calculated. If this value reaches a given threshold, the algorithm significantly lowers the time step. This algorithm ensures that the time step is sufficiently small, but not too small, assuming that the error estimation is applicable in the entire domain.

2.4.3 Quadratic Trajectory Fitting

A small issue with the time stepping algorithm is that it saves the data clustered in time steps. When working with an electron beam it would be much better to have the data points clustered in cross-sections, because then all particles in a cluster would have the same z -position and properties such as the hyperemittance would be easily obtainable. In order to find e.g. the exact focal point it therefore becomes necessary to interpolate the positional data between the time step clusters. This can be done by fitting quadratic trajectories to each particle individually. Note that this method only works well in regions with low forces.

When finding the true focal point, it is best to start by approximating a rough focal point $z = f_{rough}$ from the time dependant data. Thereafter a region is defined, $z \in [f_{rough} - \Delta z, f_{rough} + \Delta z]$, and all data points within this region are used to fit the quadratic curves. The quadratic fitting returns a series of continuous functions for which it is possible to express the emittance and the Twiss parameters as functions of z , which makes it possible to obtain the true focal point.

3

Methodology

COMSOL Multiphysics® is a simulation tool mainly used to solve FEM related physical problems. A COMSOL project starts by defining the *Geometry* of the system. Next the *Physics* and *Material* properties of the domains are defined. The system is then divided into smaller elements creating a *Mesh* and lastly the simulation is calculated with a *Study* of some sort. The words emphasised are the terms used in COMSOL to structure a model. This chapter will focus on explaining the COMSOL model and the mesh convergence procedure in detail, before discussing three additional methods to improve the COMSOL model.

3.1 Delimitations

When modeling physical systems one must select a degree of approximation in the model that is instrumental to the needs of the application and suitable for the available computational resources. More often than not it is preferable to have a semi-accurate result that can be computed in a matter of seconds than having a perfect result that takes hours. Finding the right balance is one of the key aspects. The Arcam EBM machines are very complex and modelling them identically is impossible. Certain simplifications were therefore made regarding the complexity of the model in order to ensure that the project was feasible. Explicitly stated, the delimitations of the project are the following:

- The initial electron beam will be supplied and the source will not be investigated in detail
- The electron-powder interaction will not be taken into account, only the beams hyperemittance and brightness in the powder plane
- The simulations will assume ideal conditions and will not take external parameters into account such as external magnetic fields or current fluctuations.
- The astigmatism lens will be excluded to lower the analytical complexity. The astigmatism lens is an essential part of the lens system, but because it is computationally identical to the deflection lens it can confidently be assumed to be easily implemented in future work.
- All material properties will be set to vacuum for simplicity
- COMSOL's calculations will be investigated to a feasible degree, while accepting that they cannot be accounted for in full detail.

3.2 The COMSOL model

The geometry of the system can be found in Figure 3.1. The system is encapsulated by a 1200 mm long cylinder with a radius of 200 mm. A 300 mm long cylindrical tube with a 30 mm radius surrounds the optical axis for $z \in [150 \text{ mm}, 450 \text{ mm}]$. The tube represents a stainless steel foil placed inside the chamber to shield the electrons from electric fields from the magnets, as well as protecting the surface of the column from powder residue. Both the foil and the outer column are grounded. The outer cylinder is set as the boundary for the magnetic insulation. The material properties are set to vacuum, meaning the domain has material constants permittivity $\epsilon = \epsilon_0$, permeability $\mu = \mu_0$ and conductivity $\sigma = 0$.

Surrounding the foil is the lens system. The focus lens is located at $z = 300 \text{ mm}$ and the deflection lenses at $z = 370 \text{ mm}$. The astigmatism lenses should be included at $z = 230 \text{ mm}$, but they have been left out. The aim of this project is to prove that it is possible to model the Arcam EBM lens system in COMSOL. Because the astigmatism lens and deflection lens are computationally identical it is sufficient to only model one of them in order to prove that they both are possible to model. Removing the astigmatism lens simplifies the analytical complexity and makes the project more feasible.

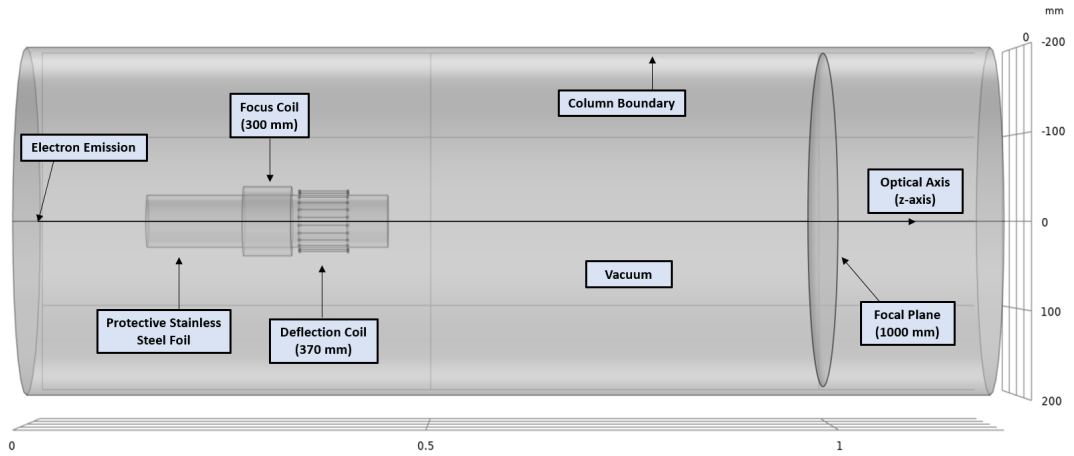


Figure 3.1: Geometry of the system.

The focus lens is a 60 mm long square toroid with an inner radius of 30 mm and an outer radius of 40 mm. The coil has 350 circular turns homogeneously distributed within its volume. The current of the coil can be varied within the interval of 3.47 A to 3.50 A to obtain a focal point at $z \in [998 \text{ mm}, 1008 \text{ mm}]$ on the optical axis.

The deflection lens is also 60 mm long and has a radius of 35 mm. It consists of 24 straight wires which are connected by 48 circle segments on the top and bottom. The geometry of the design can be found in Figure 2.8 and the currents are assigned according to equation 2.15, with $0 \leq \sqrt{I_x^2 + I_y^2} \leq 60 \times 300 \text{ mA}$. The prefactor of

60 is included so that each factor $N \sin \theta_i$ is close to the integer number of wires in the coil, meaning that the actual current passing through each individual wire is 300 mA (or less if the deflection angle is decreased).

The electron emission is released in the vicinity of the origin. The specifics of the emission can be found in Appendix A. 1000 particles were modelled with a total beam current of 10 mA. The powder surface is intended to be located in the offset plane 5 mm behind the focal plane, $z = 1000$ mm.

A magnetic field is produced when current runs through the wires of the lenses, see Figure 3.2. Specifically, 3.427 A focus current and 300 mA deflection current. The flux density is strongest in the red region in the vicinity of the lens system and weakest on the column boundary. A zero magnetic flux boundary condition is placed on the column boundary. The white streamlines follow the magnetic field and help visualize the field direction. The magnetic field can be seen to mainly follow the optical axis within the focus coil. The field is however slightly concave and this will cause a small spherical aberration. The homogeneous field in the deflection lens is perpendicular to the optical axis and pushes the field lines downwards, thereof the higher density of field lines below the lens system.

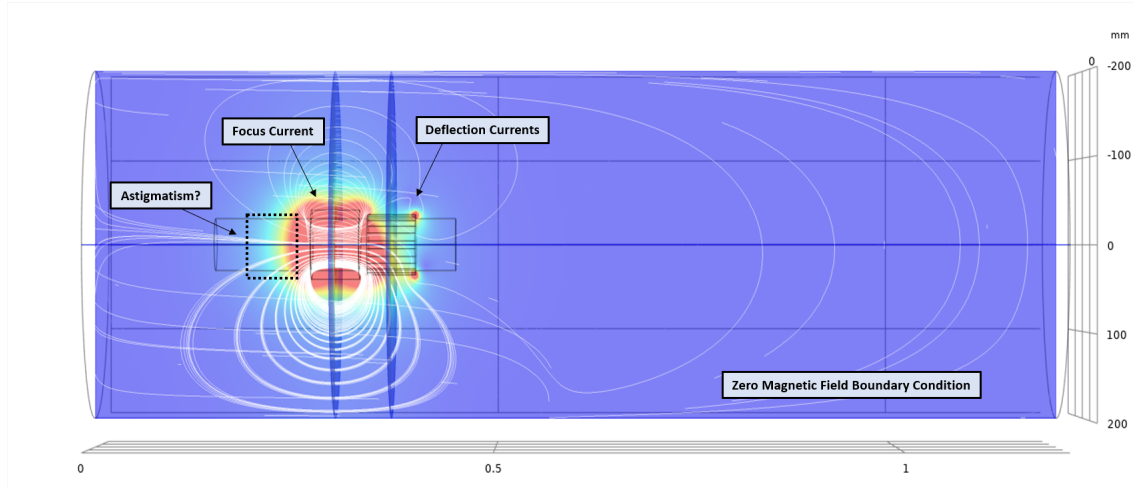


Figure 3.2: The magnetic field created by the lens system. The flux density is largest in the red regions surrounding the lens system and the white streamlines visualize the magnetic field line.

The particle trajectories of the beam propagating through the magnetic field can be seen in Figure 3.3, where the color of the beam indicates the magnitude of the magnetic force. The electrons are emitted from the source in the origin located to the far left. The beam is diverging as it approaches the lens system. The strong magnetic forces of the focus lens influence the electrons to start spiraling and forces the beam to converge. The deflection lens simultaneously deflects the beam at an angle from the optical axis. The beam reaches a focal point in the vicinity of the focal plane.

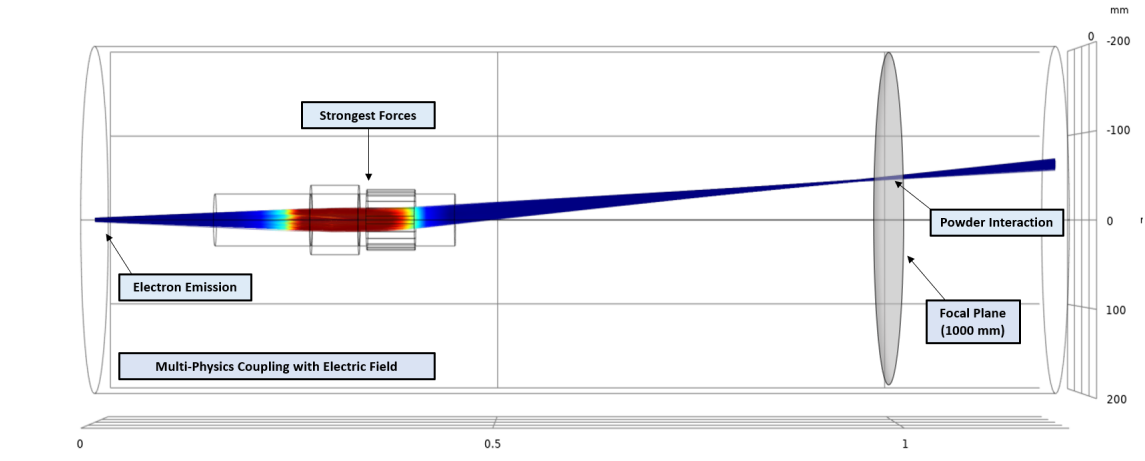


Figure 3.3: Particle Trajectories. The colors indicate the magnitude of the force exerted on the particles, which is strongest in the lens system.

Although the system is dominated by the magnetic field, another force influences the system, namely the electric force caused by the electron interaction between the electrons in the beam. The electric force will influence the particle trajectories, but it will also depend on the particle trajectories. Finding the correct particle trajectories therefore requires a steady state to be achieved. COMSOL finds this steady state by using a multi-physics coupling between the particle trajectory physics and the electric potential physics. The multi-physics coupling implies that the calculations of the two coupled physics are calculated consecutively in an iterative manner. As one physics is calculated, the other physics is considered constant. With each iteration both physics are updated and eventually a steady state system will be achieved. Specifically the multi-physics calculation starts with the particle trajectories being calculated without an electric field. Thereafter an electric field potential is calculated from the particle trajectories. The particle trajectory calculation is thereafter repeated, but now including the influence from the electric potential. A new electric potential is calculated from the updated particle trajectories and so on. This process continues until a steady state is achieved. It was found to be sufficient to calculate the multi-physics coupling with two iterations, meaning the particle trajectories and the electric potential are both calculated twice.

The electric potential can be seen in Figure 3.4. The blue regions indicate the negative potential created by the electrons. The potential obviously follows the particle trajectories and is otherwise only influenced by the grounded potential on the foil and column boundary. The electrical potential is strongest in the focal point located in the focal plane. As previously mentioned, it is preferential to place the powder plane in the offset plane a few millimeters behind the focal plane. The high electron density naturally distributed the electrons more evenly and consequently a more evenly distributed spot is achieved.

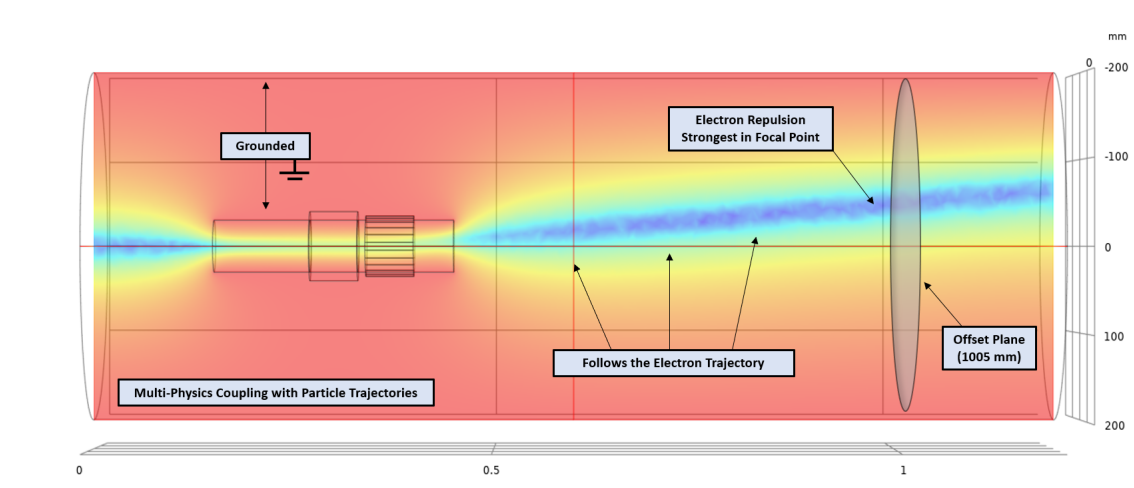


Figure 3.4: The Electric Potential created from the charge distribution of the particle trajectories.

3.3 Mesh Convergence and Model Evaluation

It is essential that the model is sufficiently resolved by the mesh. The mesh is proven to be sufficiently resolved by looking at mesh convergence. A series of models with increasing resolution are created and the results of each model are evaluated using the three convergence variables E_B , Δr and FWHM. The mesh is regarded to be converged once the result of the model remains the same even though the resolution is increased.

3.3.1 Mesh Design

When meshing the domain, the general idea is to increase the resolution in the regions where the particles propagate, focusing on the regions where the forces are the largest. The forces are largest within the lens system and therefore this is the most important region to resolve. The remaining domain is quite big and there is a large volume in which the particles never traverse. These areas should be sought to have a low resolution to lower the computational time. In order to systematically increase the resolution, while maintaining a distinction between regions of high and low resolution, a mesh design is required. The mesh design explicitly states how the meshing parameters change with each iteration in the mesh convergence. In this project three mesh designs have been investigated. The three designs are called Default, Only Foil and Foil & Intermediate and can be seen in Figure 3.5.

The entire domain is divided into three different regions. The domain inside the foil, the column surface and the intermediate domain between the foil and the column surface. Each region can be assigned individual values for the meshing parameters h_{min} , h_{max} and h_{growth} . h_{curve} and h_{narrow} were found to be unimportant and h_{max} is the most important parameter. Because the magnetic field is strongest within the foil domain, this region required the highest resolution. The Default

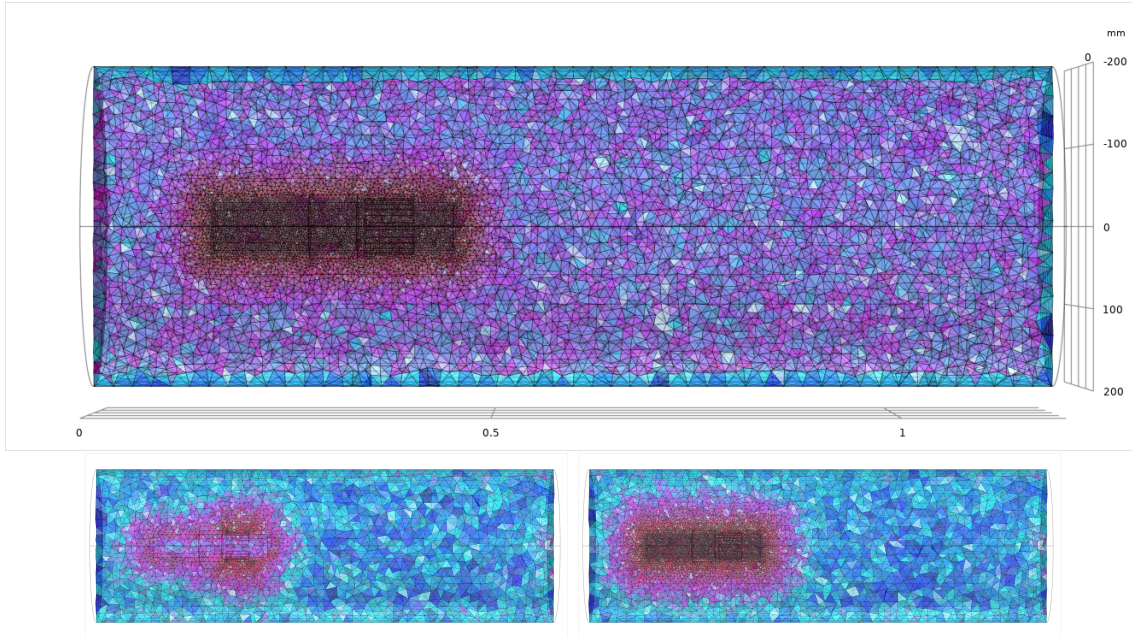


Figure 3.5: The three mesh designs: Default (bottom left), Only Foil (bottom right) and Foil & Intermediate (top).

mesh design is very simple and assigns COMSOL's default meshing values in all three regions. COMSOL provides nine default sets of meshing parameters, see table 3.1, and therefore nine different models of increasing resolution were produced using the Default design. The Default mesh design is less resolved than the two other designs and is mainly included as a benchmark. The Only Foil design increases the resolution solely in the foil region, while the Foil & Intermediate increases in both the foil and intermediate region, as can be seen in Figure 3.5.

Table 3.1: COMSOL's nine default sets of values for the meshing parameters h_{\max} , h_{\min} and h_{growth} . The values for h_{\max} and h_{\min} are given in millimeters.

	Coarsest				Normal				Finest	
h_{\max}	600	360	228	180	120	96	66	42	24	
h_{\min}	84	64.8	48	33.6	21.6	12	4.8	1.8	0.24	
h_{growth}	2.0	1.85	1.7	1.6	1.5	1.45	1.4	1.35	1.3	

It is important to clarify explicitly how the resolution is increased when seeking mesh convergence for the Only Foil Design and the Foil & Intermediate design. To avoid confusion regarding the term iteration, the term simulation number will be used to distinguish between the models in the iterative series. Each simulation number represents the specific set of meshing values used to produce the mesh, see Table 3.2. 14 models were produced for both designs. The first simulation numbers of both designs are identical and they have been given the parameter values of the finest default COMSOL values in all three regions. For the second simulation, the meshing parameters h_{\min} and h_{\max} have been decreased by 20% in the foil region for both designs and by 5% in the intermediate region for the Foil & Intermediate design.

The decrease in element size is then repeated for each iteration. For each simulation number the magnetic energy E_B , the average difference in position Δr and the FWHM of the beam at $z = 1005$ mm are concluded. The results of the convergence variables for all three mesh designs can be seen in Figure 3.6 and detailed information regarding the Only Foil and Foil & Intermediate models can be found in Table 3.2.

3.3.2 Mesh Evaluation

The Default design doesn't converge properly since the resolution is too small, but it acts as a good reference and is therefore included. Figure 3.6 shows that the Only Foil convergence series starts to converge on simulation number 5, and the Foil & Intermediate on simulation number 3, assuming simulation number 6 is an anomaly. The convergence is identified by Δr and FWHM approaching a constant value. The magnetic energy E_B turned out to be a bad convergence variable and shows no signs of convergence. Because there is a difference in the mesh convergence between the two designs, the conclusion was made that it was necessary to have an increased resolution in the intermediate region and therefore the Foil & Intermediate mesh design was chosen to be better.

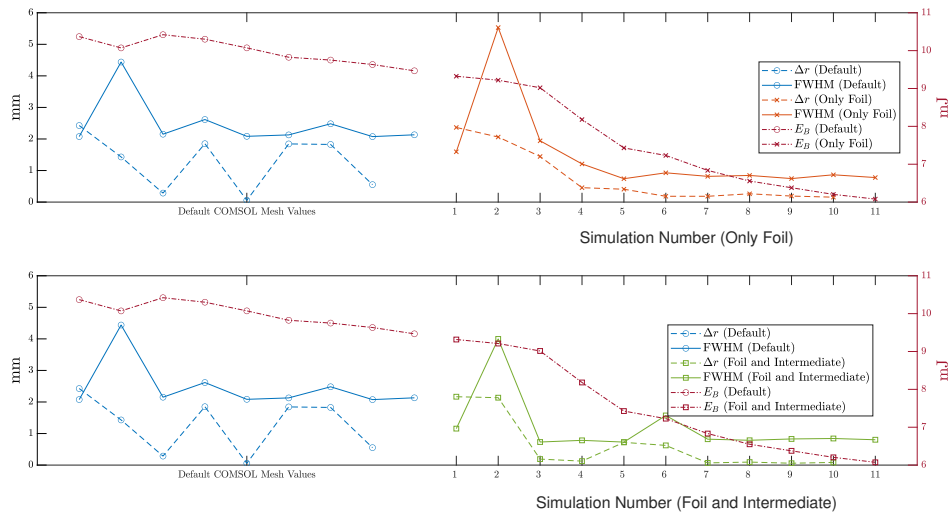


Figure 3.6: The results from the mesh convergence for the Only Foil design (top) and Foil & Intermediate design (bottom), using convergence variable Δr , FWHM and E_B . The dotted data represent the Default design in both graphs.

It is important to ensure that the model is robust. Robustness means that the results will remain the same even when the model is changed slightly. A simple way to slightly change the system is by inserting a random point. The point changes the geometry of the model, which forces the meshing algorithm to adapt. The new mesh will be different than the previous, but the resolution will remain the same. If the results change after inserting the random point it can be concluded that the results are influenced by the mesh structure. The robustness was tested for the entire Foil & Intermediate convergence series by placing points randomly along the

3. Methodology

Table 3.2: Detailed information regarding the models used in the mesh convergence test for both the Only Foil design (top) and Foil & Intermediate design (bottom)

Simulation Number	hmax (mm)		Number of Nodes	Computation Time (min)
	Foil	Intermediate		
1	19.20	24.0	40954	10.7
2	15.36	24.0	41055	8.8
3	12.29	24.0	41434	9.2
4	9.83	24.0	44480	10.3
5	7.86	24.0	49615	11.1
6	6.29	24.0	59361	10.7
7	5.03	24.0	76928	11.0
8	4.03	24.0	107726	12.9
9	3.22	24.0	162374	21.1
10	2.58	24.0	264635	35.1
11	2.06	24.0	443296	66.9
<hr/>				
1	19.20	22.8	45353	11.9
2	15.36	21.66	50517	10.9
3	12.29	20.58	56972	10.3
4	9.83	19.55	66688	10.5
5	7.86	18.57	79849	13.5
6	6.29	17.64	98476	16.1
7	5.03	16.76	126674	19.6
8	4.03	15.92	169728	26.2
9	3.22	15.13	239121	31.1
10	2.58	14.37	357912	47.5
11	2.06	13.65	556433	83.9

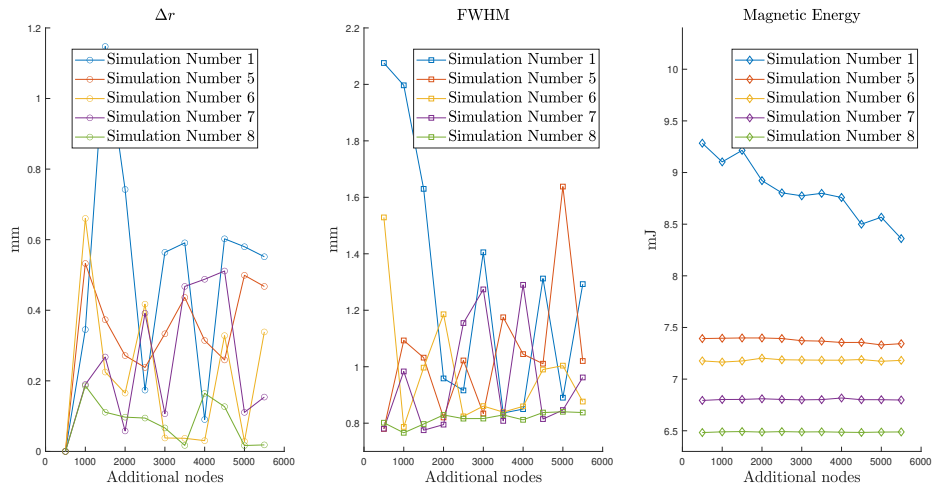


Figure 3.7: A robustness study that introduces random points (500 per iteration) in the mesh.

beam trajectory, 500 points at a time. The results for simulation numbers 5,6,7 and 8 can be seen in Figure 3.7. Simulation 1 is also included as a reference.

The results from the convergence parameters Δr and FWHM can be seen to change quite a lot. From Figure 3.6 the series seemed to converge by simulation number 3, however the series only becomes moderately robust around simulation number 8. Therefore simulation number 8 was chosen as the best model, achieving the best possible mesh convergence and robustness within a reasonable computational time. The accuracy of the mesh convergence can be quantified by looking at Δr and FWHM in Figure 3.7. The average displacement can be seen to be around $100\mu\text{m}$ on average, and the FWHM varies between 0.76mm and 0.83mm . The meshing parameters of simulation number 8 can be found in table 3.3. The results of the mesh convergence and robustness test will be discussed in detail in chapter 5.

Table 3.3: Meshing parameter values in the three regions for simulation number 8 (Foil & Intermediate). Finest Default included as reference.

	hmin	hmax	hgrowth
Finest Default	0.24 mm	24 mm	1.30
Foil Volume	0.04 mm	4 mm	1.30
Intermediate Volume	0.16 mm	16 mm	1.15
Outer Column Surface	0.24 mm	24 mm	1.30

3.3.3 Computational Time

From the mesh convergence and the robustness test simulation number 8 was concluded to be the best model. The model has a total of 1090147 elements with an average skewness of 0.6608. The simulation is calculated in two separate steps: the stationary magnetic field calculation and the particle tracing coupled together with the electric field calculation. The coupled calculation is done with two iterations. The magnetic field and the coupled particle tracing calculations take approximately ~ 5 minute and ~ 20 minute respectively using COMSOL MultPhysics 5.5 on an HP ZBook with 64 Gbit RAM and an Intel Xeon processor (E3-1535M v6) with 4 cores (8 threads).

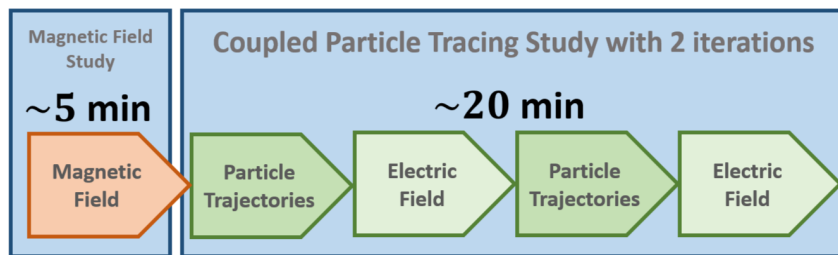


Figure 3.8: Time evaluation of simulation number 8.

3.4 Methods to reduce the computational time

3.4.1 Super-positioning the magnetic fields

The magnetic field created from a wire is completely proportional to the current. They scale 1:1. If the magnetic field has been calculated for a certain current, then the magnetic field caused by a different current can be obtained by simply rescaling the already calculated magnetic field. Additionally, magnetic fields can be super-positioned, meaning that the magnetic field for the different coils can be calculated individually and thereafter combined and scaled arbitrarily. This method will completely remove the computational time required to calculate the magnetic field.

Super-positioning the magnetic fields does introduce some potential problems regarding flexibility. The current model has vacuum everywhere, but if the material properties of the domain are not homogeneous the magnetic field will not scale proportionally everywhere. An interesting multi-physics aspect is related to the effect of the heat expansion of the coil on the magnetic field. This would require introducing the material properties of the coil. The simulation of this effect would probably become incorrect if a super-position approach was implemented.

Another problem regarding the super-positioning of the magnetic fields is the mesh. The single magnetic fields are defined by their values in the mesh nodes and super-positioning different magnetic fields may combine different meshes. For example, it could be interesting to model how the magnetic field is effected by slightly tilting a lens. To account for this the entire mesh system would have to be rotated along with the lens. This could create problems where the nodes of the different magnetic fields don't coincide. Also, some nodes lying on the boundary of the initially defined calculation space (the space for which COMSOL has been told all calculation will occur within) would end up being rotated outside of it, meaning their positions may violate initial assumptions e.g. the zero magnetic field boundary condition. This would make COMSOL crash. It is possible to account for with various constraints and interpolation, but this would require additional work and COMSOL may not support it.

3.4.2 Approximating the electric field

The electric force is small compared to magnetic force and the effect of it occurs closer to the powder plane, meaning it will have a smaller impact on the position in the powder plane, see Figures 3.2, 3.3 and 3.4. Additionally the electric force depends on the charge distribution which very much coincides with the beam trajectory. By approximating an electric potential along a predicted beam path instead of calculating it from the particle trajectories, the need for coupling can be removed, reducing the computational time substantially.

The electric potential and the electric field for a straight beam going down the optical axis can be found in Figure 3.9. The electric potential can either be approximated

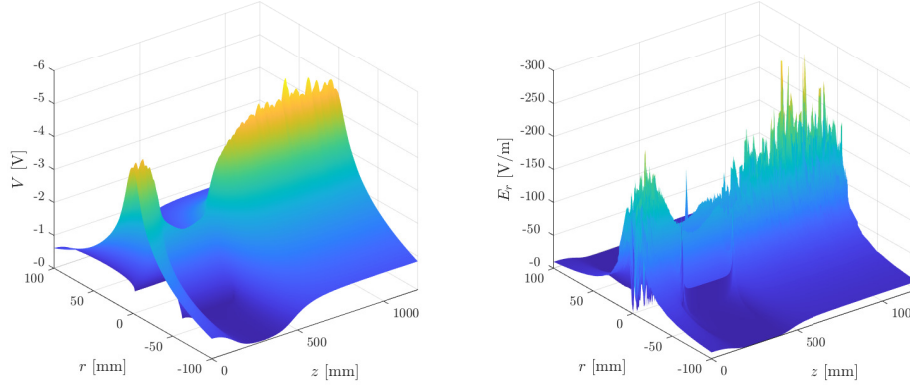


Figure 3.9: The radial Electric Potential $V(r, z)$ and the radial Electric Field $E_r(r, z) = -\nabla V$ created by a straight electron beam traversing down the optical axis. Notice how the electric potential falls in the foil region due to the foil being grounded.

as a constant potential $V(r)$ that only depends on the radial distance of the electron from the center of the beam, or it can be a slightly more advanced potential $V(r, z)$ that also takes the z -position into consideration. The radial Electric Force, see Figure 3.10 is zero within the beam and increases rapidly until $r \approx 10$ mm, whereafter it gradually dies out. Initially this may seem to violate Coulomb's law, where the force is proportional to r^{-2} , but this can be explained due to the charges cancelling within the cluster, so called electron screening. The beam radius is generally smaller than 10 mm in the post foil region, which means that the radial force can be approximated with a very simple linear function going through the origin. Furthermore, the dependence of z can be included by changing the slope of the function. Therefore, a rough but sufficiently accurate approximation of the electric potential could simply be $F_E(r, z) = k(z)r$, for some pre-factor $k(z)$.

When deflection is present it becomes slightly more complicated to approximate the radial force. However, with some linear algebra it becomes manageable. The beam trajectory will be defined by two points. $P_1 = [0, 0, 370]$ in the center of the deflection coil and $P_2 = [x_f, y_f, 1000]$ in the focal plane, where x_f and y_f are the coordinates where the beam traverses the focal plane. For a particle located at $P_0 = [x, y, z]$ the radial distance d between the particle and the beam, as well as the direction of the force \vec{f} can be calculated using the expressions in equation (3.1), where $||\vec{P}||$ is the 2-norm and \vec{P}_{AB} the vector between points P_A and P_B . Note that \vec{f} is not normalized in this expression. Using these equations the potential from a straight beam can be used to approximate the electric force for any beam. However, the success of this method depends entirely on the coordinates x_f and y_f in point P_2 being correctly predicted.

$$d = \frac{||\vec{P}_{10} \times \vec{P}_{20}||}{||\vec{P}_{12}||} \quad \vec{f} = \vec{P}_{10} - \frac{\vec{P}_{10} \cdot \vec{P}_{12}}{||\vec{P}_{10}|| ||\vec{P}_{12}||} \vec{P}_{12} \quad (3.1)$$

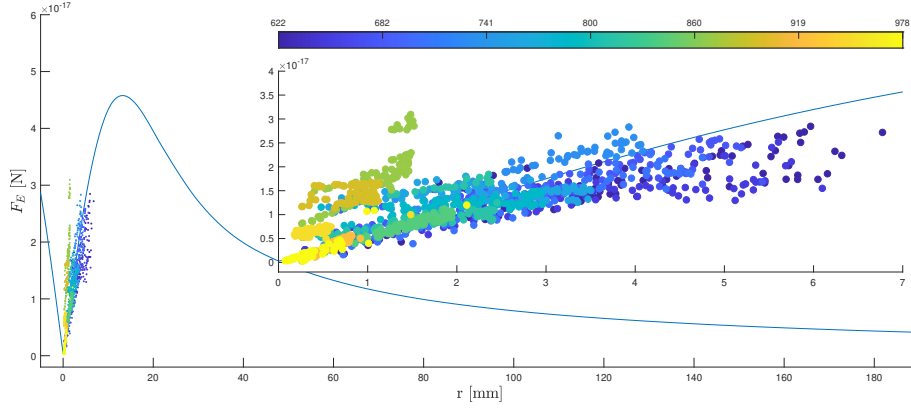


Figure 3.10: The average radial Electric Force F_E (blue line) of a straight beam can be seen to increase almost linearly up until $r \approx 10$ mm, whereafter it approaches zero slowly. The scatter plots shows the electric forces exerted on 100 particles at 14 different time steps between $z = 600$ mm and $z = 1000$ mm. The different colored clusters represent different z -positions.

3.4.3 Customizing the Time Step Algorithm

The Generalized Alpha Algorithm generally performs well, but it maybe be suboptimal in the non-foil region. In Figure 3.11 the average positional error at $z = z_i$ has been calculated for linear propagation in three different scenarios: propagating from z_i to the focal plane $z = 1200$ (blue), propagating from the emission source $z = 0$ to z_i (red) and propagating 200 mm forward of z_i (green). The electrons are propagated completely straight from their starting position with their velocity in this position. The foil region can be seen to cause the largest error when propagating linearly, and this is simply because this is where the forces are strongest. What is interesting is how small the error becomes in the outer regions. The positional error Δr is less than 0.5 mm both propagating linearly from the source at $z = 0$ all the way to $z = 250$ mm and propagating from $z = 500$ mm all the way to the focal plane at $z = 1000$ mm. This means that approximately three quarters of the optical system can be replaced with a linear propagation, that takes less than a second to compute, and the accumulated average positional error will be less than a millimeter.

The Generalized Alpha Method can be reduced to the simpler Velocity Verlet Algorithm by choosing $\beta = 0$ and $\gamma = 0.5$. Each time step is computed in three steps, see equation 3.2. First the next position \mathbf{r}_{i+1} is calculated from the current position \mathbf{r}_i , the current velocity \mathbf{v}_i and the current acceleration \mathbf{a}_i . The acceleration \mathbf{a}_{i+1} in the next position is thereafter approximated with the approximated potential field $\tilde{V}(\mathbf{r}_{i+1})$. Lastly the velocity in the next position \mathbf{v}_{i+1} is calculate from the current velocity \mathbf{v}_i and both accelerations \mathbf{a}_i and \mathbf{a}_{i+1} . The resolution will depend on how small Δt is and the computational time complexity $\mathcal{O}(\Delta t^{-1})$ will be proportional to the invers.

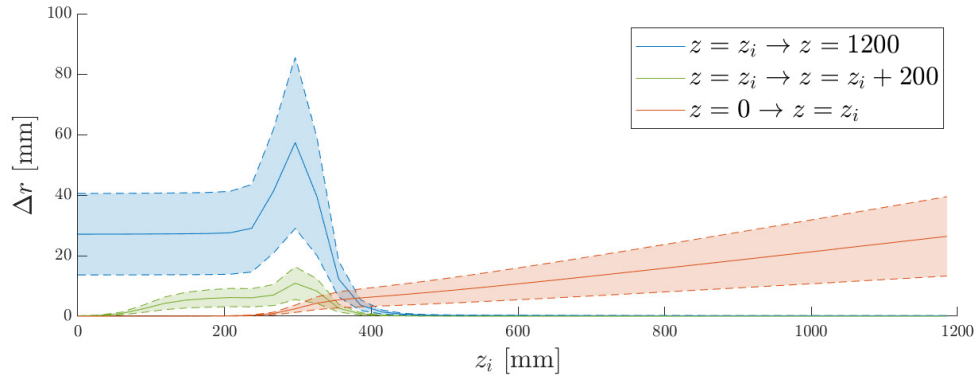


Figure 3.11: The linear propagation error accumulated propagating from, or to, the position z_i .

$$\begin{aligned}
 \mathbf{r}_{i+1} &= \mathbf{r}_i + \Delta t \mathbf{v}_i + \frac{\Delta t^2}{2} \mathbf{a}_i \\
 \mathbf{a}_{i+1} &= -\frac{q_e}{\gamma(\mathbf{v}) m_e} \nabla \tilde{V}(\mathbf{r}_{i+1}) \\
 \mathbf{v}_{i+1} &= \mathbf{v}_i + \frac{\Delta t}{2} (\mathbf{a}_i + \mathbf{a}_{i+1})
 \end{aligned} \tag{3.2}$$

4

Results

The main purpose of this project was to find out whether or not it was possible to simulate the Electromagnetic Lens System of an EBM Machine in COMSOL using either FEM or BEM. Unfortunately it was rather quickly concluded that FEM was the only viable option. It was discovered that the mathematical environment available in COMSOL, lacks the support for vector based potentials, which are necessary for BEM. Basically, this means that COMSOL could support magnetic potentials, but not currents. Furthermore, it was also concluded that COMSOL lacked the implementation of mesh free time stepping algorithms, meaning that a mesh would have been required even if COMSOL could support BEM with vector based potentials. COMSOL is currently planning on implementing both vector based potentials and mesh free particle tracing in the future, but for now FEM is the only viable option they provide.

Once established that it is possible to simulate the lens system, the following step was to optimize the model and find the optimal balance between computational time and mesh-independence. This was done by looking at mesh convergence and robustness. Three different mesh designs with different strategies for the construction of the mesh were investigated for varying decrease of resolution, see section 3.3. After testing and comparing the designs the so called Foil & Intermediate design was selected. The mesh convergence of the Foil & Intermediate design converged nicely, however when investigating the robustness it was discovered that the convergence was misleading. It was shown that the results were not robust and therefore not independent of the mesh. Simulation number 8 was chosen as the best model although $\Delta r \approx 100 \mu\text{m}$, with a FWHM varying between 0.76 mm and 0.83 mm. These variations are not good enough to make the results sufficiently reliable. Especially regarding the fact that the results of this project are stand alone, without comparison to results from real data or other simulations.

The FEM method in COMSOL proved to be able to calculate the magnetic field, the electric field and the particle trajectories for simulation number 8 in about 25 minutes, given the computational capacity previously specified. This makes it possible to compute roughly 50-60 different simulations within 24 hours. This creates a new discussion regarding computational time: At what point does the simulation software become fast enough? This is a highly subjective question without a general answer. The question is however still very important and it will therefore be further discussed in the next chapter. Another important result obtained from the time evaluation is the division of computational time between the different calculations,

see Figure 3.8.

Three external methods have been proposed to improve the simulations in COMSOL. All three have been shown to be successful in lowering the computational time, but they also place constraints on the model in one way or another. The superposition of the magnetic fields works as expected, completely removing magnetic field calculation, and can be implemented within the COMSOL framework. The downside of the super-positioning is mainly that it constrains the material properties of the model to only be a homogeneous vacuum. If it is desired to simulate effects including other material properties, which it likely is, this method may be completely useless. Besides this, issues could arise regarding the geometry of the mesh if it is desired to test issues related to angular displacement of the lenses. The magnetic fields can easily be scaled with regard to the currents, but it can not as easily be rotated and displaced. It is unknown how COMSOL will handle the super-position of two differently meshed magnetic fields or how it will handle a mesh that does not comply with the general geometry of the model.

The approximated electric field potential turned out to be quite good given that fact that it is a only simple linear approximation. Also the simplified time stepping algorithm proved to be quite successful. The results of the approximated electric field combined with the external Velocity Verlet time stepping is visualized in Figure 4.1 and the details regarding the accuracy can be seen in Table 4.1. The figure shows the hyperemittance in the focal plane and the offset plane, with and without deflection. Three data points are included: the true data obtained from the COMSOL simulation, linearly propagated data obtained from propagating the true data linearly from $z = 600$ mm, and the Velocity Verlet data. The Velocity Verlet data is propagated the same distance as the linear data. The propagation was made as described by equations 3.2, where the acceleration only depends on the approximated electric force $F_E = -\nabla\tilde{V}(r) \approx kr$, with $k = 1.8595 \times 10^{-16}$, seen in Figure 3.10. The calculations were run with 100 time steps ($\Delta t = 0.1$ ns), but the time step calculations showed convergence even at 15 time steps. The data points can be seen to group together in Figure 4.1, showing that all three methods achieve approximately the same result. Looking at the numbers in Table 4.1 the average positional displacement can be seen to be about 50 μm for the linear propagation and 20 μm for the velocity verlet propagation, without deflection. The approximated electric field and the velocity verlet time stepping has therefore shown to reduce the error by about 60 % compared to simple linear propagation. All three data sets obtain the same FWHM value within a 50 μm interval. These results are similar even when replacing the particle propagation in the post foil region. The decrease in accuracy can be regarded as non-existent when compared to the general accuracy of the model obtained from the robustness test, which concluded that $\Delta r \approx 100$ μm and $\text{FWHM} \in [0.76 \text{ mm}, 0.83 \text{ mm}]$.

Similar results were obtained when including deflection, although the error increased almost threefold. The increased error can be explained by the increase of magnetic field strength in the post foil region and by the simplicity of the linear algebra im-

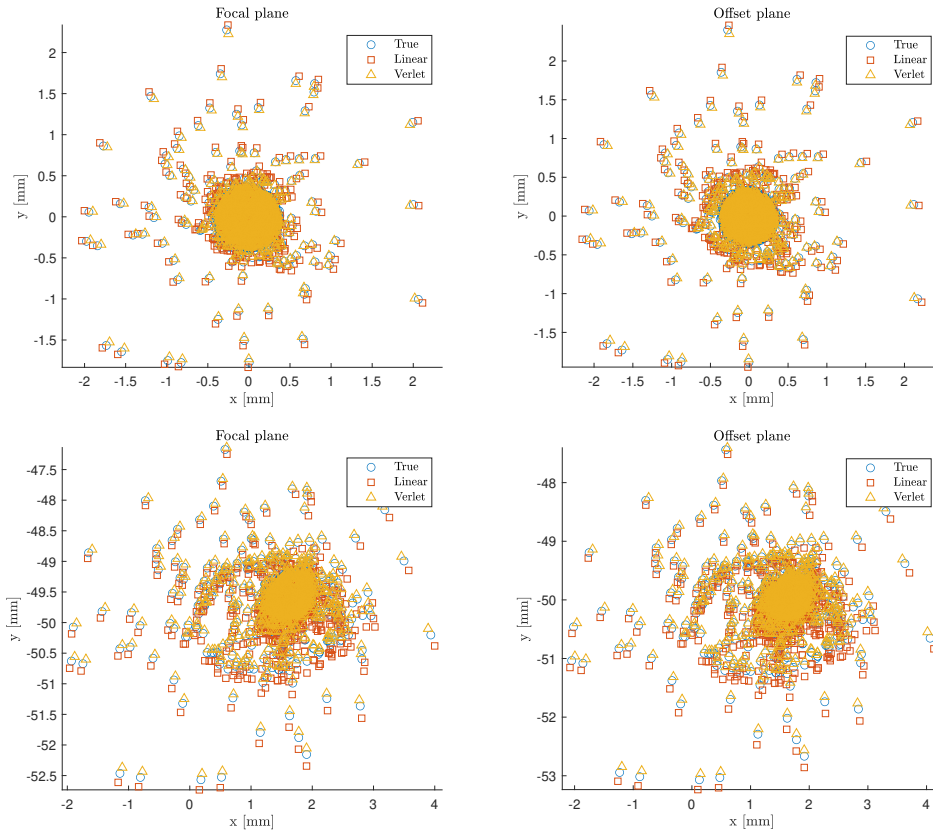


Figure 4.1: Hyperemittance in the focal and offset planes for the true, linear and for the Velocity Verlet time step propagation, both with and without deflection.

plemented to correct the direction of the force. Because the deflection lens is located further along the optical axis it increases the magnetic field strength substantially in a small region beyond $z = 600$ mm. The Velocity Verlet algorithm only accounts for the approximated electric force and does not account for the magnetic force. It is therefore probably preferred to decrease the distance propagated by the Velocity Verlet algorithm when including deflection. The linear algebra implemented to correct the direction of the force is very simple and it was never tried against any other method. It is possible that it is not sufficiently good. When investigating how the data points are grouped in Figure 4.1 it can be seen that the Velocity Verlet data points tend to be closer to the center of the spot than the true data without deflection. This trend can not be seen when including deflection. Instead the Verlet data points tend to be above the true data, in other words the Verlet points tend to be less deflected than the true data. This is probably a consequence of indirectly removing the magnetic force when switching to Velocity Verlet propagation. It could also be a consequence of the force direction correction not being sufficiently advanced.

The simplified time stepping algorithm only takes a couple of seconds to compute together with the approximated electrical potential. The computational time can therefore potentially be lower substantially. A final simulation model implementing

Table 4.1: Average positional displacement Δr and FWHM ,for short and long axis, for the hyperemittance in the focal and offset plane for the true propagation, the linear propagation and the velocity verlet propagation.

		<u>Without Deflection</u>		<u>With Deflection</u>	
		Δr (μm)	FWHM (mm)	Δr (μm)	FWHM (mm)
<u>Focus</u>	True	-	[0.79, 0.80]	-	[1.24, 1.33]
	Linear	47.68 ± 15.93	[0.80, 0.81]	138.28 ± 33.56	[1.26, 1.36]
	Verlet	18.98 ± 7.70	[0.77, 0.77]	48.10 ± 27.80	[1.20, 1.33]
<u>Offset</u>	True	-	[0.83, 0.84]	-	[1.30, 1.40]
	Linear	48.73 ± 16.25	[0.85, 0.86]	140.46 ± 34.36	[1.32, 1.44]
	Verlet	19.44 ± 7.87	[0.80, 0.81]	48.99 ± 28.18	[1.26, 1.40]

all three additional methods was never fully assembled, and therefore it becomes difficult to estimate their decrease in computational time. Assuming that no additional complications occur when assembling the model, it is estimated that the computational time could be reduced to less than 5 minutes. This is a fivefold decrease in computational time compared to not implementing any additional methods, making the simulation a lot faster. Once again this is only an estimation and the full model must be assemble before it can be verified.

5

Conclusions and Recommendations

This chapter will start by describing the difficulties regarding mesh convergence. A couple words regarding the additional methods will be mentioned before discussing the requirements of a "sufficiently fast" simulation tool, concluding an evaluation of the simulation tool created in this project. Several recommendations regarding future work will be made throughout the texts.

5.1 Discussion

The project was designed to exclude any comparison with real data in order to 1) minimize the number of factors that could cause the project to fail and 2) to avoid patent/immaterial rights issues related to publishing confidential material. For these reasons the geometric dimensions in the model were chosen to be inexact, differing slightly from the actual values of the lens system. This of course limits the possibilities for this project to make comparisons to measured results on real data or data from other software. The general strategy was to build a simulation model of a simpler system in order to investigate the numerical methods, the convergence problem and the impact of possible approximations. The dimensions of the model could then in future work be adapted to the real dimensions of the lens system and the results could be compared to real data.

The task of creating a fully converged model was at first thought to be quite simple. It turned out to be the opposite. It became clear that there are many different ways to design a mesh and too many factors that come into play. The more complicated the mesh design becomes, the harder it is to evaluate how well it performs and even harder to evaluate how accurate it is. Additionally it takes quite a lot of time to calculate the simulations which made it impossible to brute force convergence. A lot of time was spent trying to understand COMSOL's meshing algorithm and the tools offered to control the mesh. A couple of different approaches were investigated, but eventually it was realized that the customized meshing designs rarely outperformed COMSOL's own algorithm. Therefore the choice was made to use a very simple meshing structure that would give COMSOL's own algorithm as much freedom as possible while focusing on the refinement of the foil region. This resulted in the Only Foil and Foil & Intermediate designs, see Figure 3.5. Both designs showed conver-

gence when increasing the resolution, but the increase in resolution also contributed to a large increase of the computational time. The growth in computational time increased the calculation time to an extent where the models became unusable before they properly converged. Properly converged implies obtaining a robust model.

The problem of mesh convergence is one of the biggest obstacles to overcome in order to produce a simulation model able to simulate the lens system. The quick solution to circumvent the problem of mesh convergence is to switch to a numerical method without the need for the mesh structure, namely the Boundary Element Method. Solving the mesh convergence problem for a FEM model would probably require an extensive investigation among the possible configurations of a mesh structure. Other mesh elements, e.g. cubes, could be investigated and the domain could be divided in more complex ways, to name a few possible directions.

To decrease the computational time, three approaches were studied, namely superpositioning of the magnetic field, approximation of the electric field, and simplification of the time step algorithm. All these approaches showed promising results for decreasing the computational time while maintaining the accuracy. The main problem with all three methods is that they decrease the flexibility and simplicity of the model. Having a low flexibility is not necessarily a bad thing. It depends on what the simulation model will be used for. If GE decides to further pursue a simulation tool they should really evaluate what they desire to use it for. If they want a flexible model that can incorporate a bunch of different physics it is probably smart to use COMSOL as much as possible and focus on using their methods. If instead they want to calculate very specific configurations under controlled circumstances it may be smart to simply use COMSOL to learn where approximations can be made, and thereafter build a time-stepping algorithm completely independently of COMSOL.

Another problem with pre-calculating the electric potential is the risk of increasing the bias of the simulations. The main purpose of simulating something is to find out what happens. Approximations are very helpful for decreasing the computational demand, but it is important to control how they impact the results. For the approximation to be used in practice some measurement of accuracy should be created to control that the approximation doesn't alter the results in any negative way. For example, the charge distribution could be computed at random points along the beam and compared to the potential of the approximation to check that they match. Furthermore, when evaluating the results of the deflected beam it becomes apparent that the system lacks an astigmatism lens. The difference in FWHM on the long and short axis is a direct result of the beam trajectory not being orthogonal to the focal/offset planes. With an astigmatism lens this phenomenon could possibly be corrected, but it would also potentially destroy the radial symmetry in the electric potential.

For future work it is important to investigate BEM once it is available in COMSOL. It is my understanding that there is a demand for BEM on the market and that COMSOL is working to implement vector based BEM and mesh-free particle

tracing. An interesting idea could also be to combine FEM and BEM in some way, allowing the two methods to complement each other. One way this could be done is by using FEM in a small domain surrounding the lens system where the forces are large, while using BEM on the rest of the domain where the forces are sufficiently small. Otherwise I would say that the most promising area to explore is external particle tracing. COMSOL gives the user a lot of freedom to try different geometries in the lens system and calculating what effects they have on the magnetic field, but the particle tracing is just too expensive to compute currently. Therefore it may be of interest to let COMSOL calculate the magnetic field, but not the particle tracing. By extracting the magnetic field a sufficiently advanced time stepping algorithm could propagate the electrons independently. This would give the user the maximum amount of freedom to play around with the material, geometry, heat expansion, etc in the model, while still maintaining a cheap time stepping calculations. There is also lot of potential to investigate a more advanced approximation of the electrical potential. The z-dependence could be taken into account, as well as the magnetic attraction between the electrons.

5.2 How fast is fast enough?

How fast must a simulation tool be to be useful? This is a very hard question to answer. At least if you seek a more specific answer than "the faster the better". To attempt to answer this question, I would like the reader to try and put themselves in the shoes of an engineer in the Research & Development department. Let's say the company just recently released an upgraded lens system to their machines and the first customers got their machines upgraded last week. Reports are coming in that the upgraded machines are malfunctioning and the electron beam is deviating from its predicted path. You are assigned the task to fix this malfunction. You know that time is of the essence since the customers are losing a lot of money with their production being offline. What do you do? Well, there are plenty of possible reasons for why the machine could malfunction. The lens system could be slightly tilted, the currents could be smaller or larger than expected, an external magnetic field could be effecting the beam, the lens could be deformed due to heat expansion, there could be something wrong with the cathode, etc etc. A skilled engineer will typically know which scenario's are more likely than others. However, the engineer will still be required to acquire a physical machine, reinstall the lens system and run a series of tests to conclude what the cause may be. This takes a lot of time. It takes several hours just to pump vacuum into the chamber and often several days to build an actual object.

This is when a simulation tool capable of modelling the lens system becomes extremely valuable. With it the engineer could test a hypothesis quickly and remotely and a lot of time and resources could potentially be saved. The engineer would load the lens design into the model and could alter it in accordance to the hypothesis. Thereafter a series of parameter sweeps could be run and the results could be compared to the recordings of the malfunction. Hopefully the simulations will identify

the cause of the problem, but if not it will still provide valuable information on which hypothesis is less likely to be the cause.

So, how fast must the simulation tool be? Well, imagine yourself working on a problem. Once you have an idea you want to check it right away. If you can't check it right away you are forced to write down and organize your thoughts and plans. If not you might forget what it is you are actually looking for when presented with the results. This effect increases as the number of ideas you wish to test increases. What I am trying to say is that it is not enough to say that a faster tool is a better tool. For the tool to be efficient it must be fast enough to provide a fluent and friction free problem solving environment. Only when the program is able to provide instant feedback, can it be considered to be perfect.

Personally, having worked with simulation throughout this project, I would have liked a computational time no longer than a minute for a rough calculation. That way an engineer can use the program fluently, trying out different settings and specifications and seeing how the model responds. Once the desired settings have been identified a longer calculation becomes desirable either increasing the accuracy substantially or by sweeping over a number of parameters. With a computational time of 20-30 minutes I found it very frustrating to achieve continuity. I would often spend several hours running the same calculation over and over again without obtaining any new information. There was a constant time pressure where I felt that I was wasting time when I didn't run a simulation, and ultimately this resulted in me running a bunch of unnecessary simulations. I mainly struggled with this when investigating mesh convergence. The mesh convergence required a large number of simulations to be run and would often be done over night. This means it would take at least a day to test an hypothesis. The extensive amount of possibilities regarding mesh design made it impossible to control every parameter of the model, if each parameter took a day to control. The long computational time will only become justifiable if the accuracy is unquestionable. However, as was shown in the robustness study, the accuracy in this model is not good enough.

5.3 Conclusion

It has been shown that COMSOL Multiphysics® is capable of simulating the lens system of an Electron Beam Manufacturing 3D printer using the Finite Element Method. However, in order to increase the utility of the simulation tool, the computational time must be low enough to enable instant feedback. The cost of instant feedback may be a reduced accuracy, but this is a cost worth paying when mainly investigating trends and not quantifying results. If an instant feedback is impossible to achieve a slower simulation model may be utilizable if the results are reliable enough to justify the long computational time. The model presented in this project was a first effort to investigate and evaluate the capabilities of COMSOL for the specific application. Although the model requires considerable computational time, the results showed that further work can provide valuable improvements. With additional methods, the computational time has been shown to be decreaseable at the

cost of flexibility and simplicity. There is therefore potential to create a simulation tool capable of doing sufficiently fast calculations for highly constrained models.

Bibliography

- [1] CPO software website; 2020. Available from: <https://www.electronoptics.com>.
- [2] Opera software website; 2020. Available from: <https://www.3ds.com/products-services/simulia/products/opera/>.
- [3] Rose HH. Geometrical charged-particle optics. Springer series in optical sciences. 142; 2012. Available from: <http://search.ebscohost.com/login.aspx?direct=true&AuthType=sso&db=edsbvb&AN=edsbvb.BV040803013&site=eds-live&scope=site&custid=s3911979&authtype=sso&group=main&profile=eds>.
- [4] Ridenour LN. Cathode Ray Tube Displays, Figure 8.26c. McGraw-Hill Book Company; 1948.
- [5] Benaroya R, Ramler WJ. Deflection coil for an external accelerator beam. Nuclear Instruments and Methods. 1961;10:113 – 120. Available from: <http://search.ebscohost.com/login.aspx?direct=true&AuthType=sso&db=edselp&AN=S0029554X61800906&site=eds-live&scope=site&custid=s3911979&authtype=sso&group=main&profile=eds>.
- [6] Rylander T, Bondeson A, Ingelström P. Computational electromagnetics. Texts in applied mathematics: 51. Springer; 2013. Available from: <http://search.ebscohost.com/login.aspx?direct=true&AuthType=sso&db=cat07470a&AN=clc.6e5b7ec46ff64f429707304e6081fddd&site=eds-live&scope=site&custid=s3911979&authtype=sso&group=main&profile=eds>.
- [7] Chung J, Hulbert GM. A time integration algorithm for structural dynamics with improved numerical dissipation: The generalized- α method. Journal of Applied Mechanics, Transactions ASME. 1993;60(2):371–375.

A

Electron Source Specifications

The electron source given in this project was made using BEM calculations in Opera. The data contains 10000 particles with initial positions and velocities, see their distributions in figure A.1. The initial positions are normally distributed on a disc with a 2mm radius in the $z = 0$ plane. The initial velocities v_x and v_y are also normally distributed and about two orders of magnitude smaller than v_z which is about half the speed of light. Also found in the figure is the initial solid angle Ω which is calculated using equation (A.1).

$$\Omega = 4\pi \sin^2\left(\frac{\phi}{2}\right) \quad \phi = \arctan \frac{v_r}{v_z} \quad (\text{A.1})$$

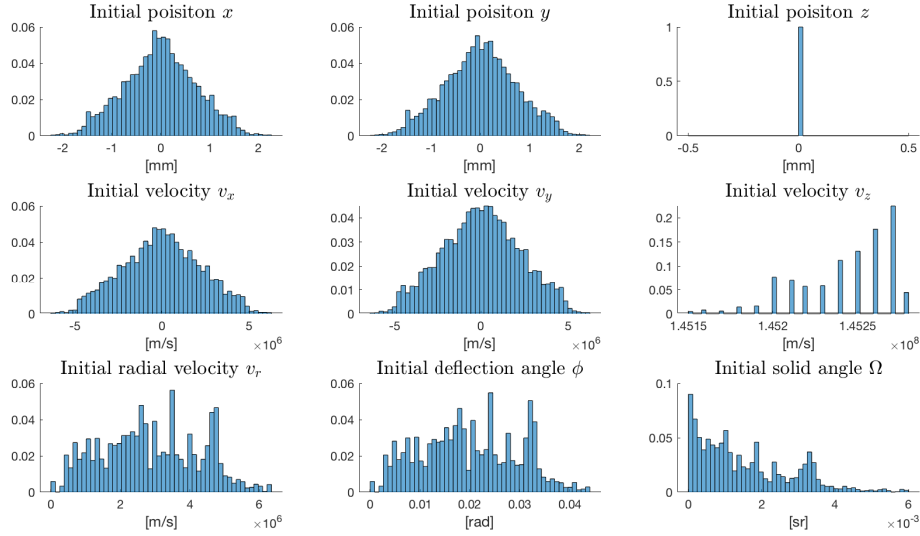


Figure A.1: Histogram of the initial position and velocity of the electron source.